

## Review

# Theranostics based on AIEgens

Dong Wang<sup>1,2,✉</sup>, Michelle Mei Suet Lee<sup>2</sup>, Wenhan Xu<sup>2</sup>, Ryan Tsz Kin Kwok<sup>2</sup>, Jacky Wing Yip Lam<sup>2</sup>, Ben Zhong Tang<sup>1,2,✉</sup>

1. Center for AIE Research, College of Materials Science and Engineering, Shenzhen University, Shenzhen 518060, China.
2. Hong Kong Branch of Chinese National Engineering Research Center for Tissue Restoration and Reconstruction, Department of Chemistry, Institute of Molecular Functional Materials, State Key Laboratory of Neuroscience, Division of Biomedical Engineering, and Division of Life Science, The Hong Kong University of Science and Technology, Clear Water Bay, Kowloon, Hong Kong, China.

✉ Corresponding authors: Dr. Ben Zhong Tang, Department of Chemistry, The Hong Kong University of Science and Technology, Clear Water Bay, Kowloon, Hong Kong, China; Tel: +852 23587375; E-mail: tangbenz@ust.hk; Dr. Dong Wang, College of Materials Science and Engineering, Shenzhen University, Shenzhen 518060, China; Tel: +86-0755-86713941; E-mail: wangd@szu.edu.cn

© Ivyspring International Publisher. This is an open access article distributed under the terms of the Creative Commons Attribution (CC BY-NC) license (<https://creativecommons.org/licenses/by-nc/4.0/>). See <http://ivyspring.com/terms> for full terms and conditions.

Received: 2018.06.10; Accepted: 2018.08.02; Published: 2018.09.09

## Abstract

The utilization of luminogens with aggregation-induced emission (AIE) characteristics has recently been developed at a tremendous pace in the area of theranostics, mainly because AIE luminogens (AIEgens) hold various distinct advantages, such as good biocompatibility, excellent fluorescence properties, simple preparation and modification, perfect size of nano-aggregation for enhanced permeability and retention effect, promoted efficiencies of photodynamic and photothermal therapies, efficient photoacoustic imaging, and ready constructions of multimodal imaging and therapy. Significant breakthroughs and developments of theranostics based on AIEgens have been achieved in the past few years, and great progress has been witnessed in many theranostic modalities, indicating that AIEgens remarkably complement conventional theranostic materials and promote the development of theranostics. This review provides theoretical insights into the advantages of AIEgens in theranostics, and systematically summarizes the basic concepts, seminal studies, recent trends and perspectives in theranostics based on AIEgens. We believe that AIEgens would be promising multifunctional theranostic platforms in clinical fields and facilitate significant advancements in this research-active area.

Key words: AIEgens, fluorescence imaging, photoacoustic imaging, cancer therapy, antibiosis

## Introduction

Theranostics, which allow the ingenious integration of diagnostic imaging capability with therapeutic intervention in a single formulation within spatial colocalization, have aroused increasing attention in both research and clinical fields [1-3]. The utilization of theranostics enables the detection of targets, monitoring of drug distribution and the evaluation of therapeutic responses, through which various functionalities can be realized, such as maximization of therapeutic efficacy, optimization of drug safety, improvement of pharmacokinetics, as well as assisting in streamlining the drug development process [4,5]. Therefore, theranostics are expected to be effective approaches to achieve the transition from conventional medicine to contemporary personalized and precision medicine [6].

Until now, various theranostic systems have been explored, involving different modalities of diagnosis (fluorescence imaging (FLI), photoacoustic imaging (PAI), magnetic resonance imaging (MRI), computed tomography (CT), positron emission tomography (PET), etc.) and therapies (photodynamic therapy (PDT), photothermal therapy (PTT), radiation therapy (RT), gene therapy (GT), chemotherapy (CHT), etc.) (**Figure 1**) [7-9]. These modalities are associated in accordance with specific needs, exhibiting the types of one (diagnostic imaging)-to-one (therapy), one-to-many, many-to-one and many-to-many. Among them, the development of multi-modalities of diagnostic imaging or therapy is attracting increasing interest, because different modalities are able to compensate for each other and

provide enhanced imaging quality and/or therapeutic efficacy. Taking FLI and MRI as examples, the use of FLI-MRI combination imaging can integrate the advantages of FLI (non-intrusive, high sensitivity, simple operation, multi-color detection and non-radioactive) with that of MRI (high spatial resolution and unlimited tissue penetration depth) in a single platform, meanwhile, their respective drawbacks (low tissue penetration and low spatial resolution for FLI; low sensitivity and time-consuming for MRI) are significantly complementary.

Selection of materials should be considered prior to designing appropriate theranostic agents. A variety of materials, in particular nanomaterials, have been employed as theranostic platforms, such as quantum dots [10], Au/Ag nanoparticles (NPs) [11, 12], carbon-based nanomaterials (nanotube, graphene) [13], magnetic NPs [14], polymeric NPs [15], and mesoporous NPs [16]. Although most of these conventional theranostic agents are effective and

widely used in both research and clinics, they have some respective and collective drawbacks including poor biocompatibility, complicated fabrication, as well as unsatisfactory outcome in terms of both diagnostic imaging and therapy.

In this context, the use of materials having aggregation-induced emission (AIE) characteristics in theranostics has recently been developed at a tremendous pace and attracted global interests in the past few years (Figure 2) [17,21,22]. Compared with some of the conventional theranostic materials including quantum dots, carbon-based nanomaterials and inorganic NPs, AIE luminogens (AIEgens) hold various distinct advantages, such as good biocompatibility, excellent fluorescence properties (in terms of strong emission in aggregates, high photobleaching threshold, great tolerance for any concentration, large Stokes shift, and turn-on feature for detecting analytes), simple preparation and modification, perfect size of nano-aggregation for enhanced permeability and retention (EPR) effect,

promoted efficiencies of photodynamic and photothermal therapies, efficient photoacoustic imaging, and facile constructions of multimodal imaging and therapy [19,23-29]. Significant breakthroughs and developments of theranostics based on AIEgens have been achieved in the past few years. On the other hand, some deficiencies of AIEgens were also revealed in theranostic applications. For instance, the working concentration of AIEgen-based theranostic platforms is generally high, making AIEgens unfavorable for *in vivo* or clinical trials. It is believed that AIEgens could be complementary to the conventional theranostic materials, and the development of AIEgens would remarkably promote the advancement of theranostics. Viewing the extremely fast growth and great significance of theranostic studies based on AIEgens, it is significantly important to publish a comprehensive review article providing theoretical insight into the advantages of AIEgens in theranostics, and introducing the basic concepts, seminal studies, recent trends and perspectives.

In this review article, we try to offer an integrated picture through



Figure 1. Some of the key imaging and therapy methods in theranostics.

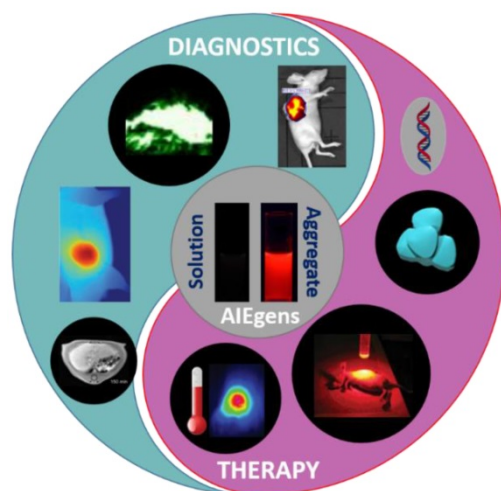


Figure 2. Theranostics based on AIEgens. Some of the key diagnostics (including FLI, PAI, IR thermal imaging and MRI) and therapies (including gene therapy, CHT, PDT, and PTT) of multifunctional AIEgens. Some elements are adapted with permissions from [17], copyright 2016 Wiley-VCH; adapted with permissions from [18], copyright 2017, American Chemical Society; adapted with permissions from [19], copyright 2015, American Chemical Society; and adapted with permissions from [20], copyright 2016, Wiley-VCH.

the introduction and discussion of representative AIE systems in theranostic studies. We will first convey mechanistic insights into the advantages of AIEgens in theranostics, on the basis of experimental measurements and theoretical simulations. Then, we introduce the classification, and highlight the new breakthroughs and trends in the area that have most recently appeared until 2018.

### Advantages of AIEgens in theranostics

Compared with many other imaging modalities, FLI has been extensively utilized and undergone an explosive development in bio-imaging applications, due to its non-intrusive, high sensitivity and simple operation features. However, conventional fluorophores usually suffer from a common photophysical phenomenon named aggregation-caused quenching (ACQ). Conventional fluorophores emit strongly in solution phase; however, they are either weakly emissive or non-emissive at high concentration or in an aggregation state (see the example of FITC in **Figure 3**) [19]. ACQ phenomenon

remains the major barrier to implementing their practical applications in bio-imaging. As an anti-ACQ phenomenon, AIE was first coined in 2001 by Tang's group [23] and refers to a unique phenomenon where some fluorophores with twisted conformations are weakly emissive in solution but become intensely fluorescent in aggregates (see the example of TPE in **Figure 3**) through the mechanism of restriction of intramolecular motion. Numerous AIEgens have been prepared, which display emission colors covering the whole visible range even with extension to the near-infrared (NIR) region (**Figure 4**) [30,31]. The AIE features not only permit their usage at high concentration or in aggregation states with bright fluorescence and high photobleaching threshold, but also enable the development of fluorescent "light-up" bio-probes responsive to external stimuli or microenvironment changes for bio-sensing and -imaging applications. Therefore, AIE has provided an array of possibilities with great potential for FLI-involved theranostic systems.

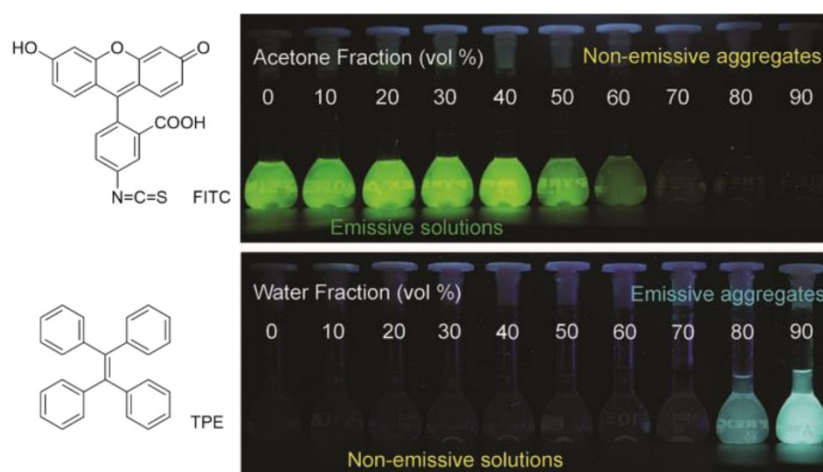


**Figure 3.** (Top) Structure of FITC and fluorescence photographs of its solution or suspension in alkaline water/acetone mixtures with different acetone fractions. (Bottom) Structure of TPE and fluorescence photographs of its solution or suspension in THF/water mixtures with different water fractions. Reproduced with permission from [21], copyright 2017 Elsevier.

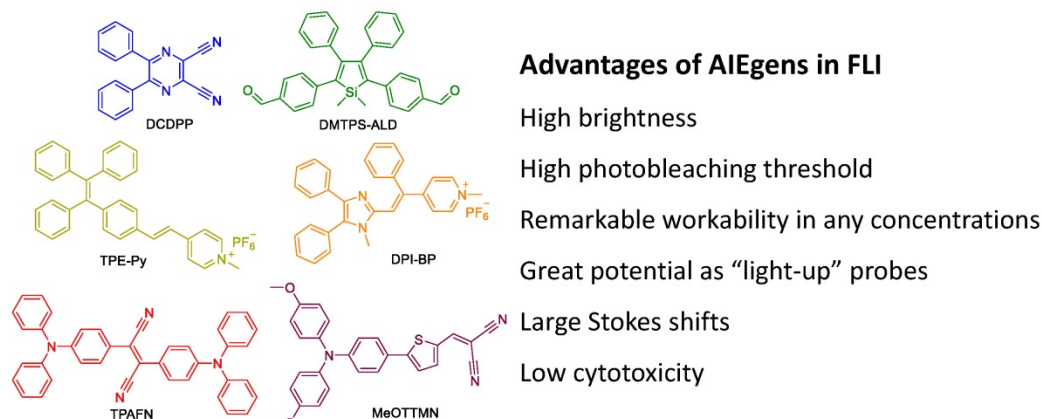


**Figure 4.** Typical AIEgens (DCDPP [32], DMTPS-ALD [33], TPE-Py [34], DPI-BP [35], TPAFN [36], MeOTTMN [37]) with different emission colors covering the whole visible range and extending to the NIR region, and advantages of AIEgens in FLI.

It is generally believed that AIEgens are a unique type of molecule suitable for PAI, particularly when they exist as single molecular species. The free rotation and/or vibration of AIEgens facilitates non-radiative decay, which can remarkably generate heat energy, resulting in them being good candidates for PAI [38]. In addition, the localized heat from photon energy generated by AIEgens further provides the opportunity for tumor ablation, which is known as PTT. PAI associated with PTT has been recently exploited and proven to be a powerful strategy for accurately probing tumor location, as well as effectively inhibiting tumor growth with minimal side effects to normal tissue. For fluorescence study, AIEgens should be used as aggregates, in which the restriction of such movements enables their excellent fluorescence properties. In contrast, for PAI/PTT application, AIEgens should be used in molecular state, and thus the energy dissipated from non-radiative decay can be efficiently utilized. In addition, some AIEgens-based nano-aggregates are in disordered amorphous form with loose packing, where molecular motions are still active, leading to high efficacies for PAI/PTT applications. It has also been demonstrated that nano-aggregates of compounds containing additional rotors obviously exhibit superior photoacoustic and photothermal signals than that of the analogue with fewer rotors [17,39]. Evidently, AIEgens having inherent rotor-like twisted structure, strong absorbance at long wavelength and amorphous properties in the nano-aggregation state, could be extraordinary agents for PAI/PTT-involved theranostics. Fluorescence and PAI/PTT pathways are indeed conflicting, and fluorescence output has to be partially or totally abandoned when the aim is to promote PAI/PTT properties.

As a non-surgical and less invasive process for cancer therapy, PDT has gained increasing attention

from both researchers and physicians, and has been clinically approved for eliminating malignant tumor cells with minimal invasiveness and precise controllability [40-43]. In PDT applications, cancer cell apoptosis or cell death is synergistically triggered by deregulation of protein functions and oxidative modification of cellular macromolecules, which are induced by reactive oxygen species (ROS). Consequently, efficient ROS generation by photosensitizers (PSs) is crucial for PDT applications. AIEgens have been recently proven to be extremely efficient ROS generators as aggregates. As depicted in **Figure 5**, AIEgens enjoy restriction of intramolecular motion upon aggregation, which minimizes loss of excited energy through non-radiative decay. Meanwhile, relaxation of the excited state is dominated by both fluorescence and intersystem crossing (ISC). In this process, the increased energy transferring from singlet state to triplet state would dramatically benefit the production of ROS, further promoting PDT applications. ROS generation enhancement in aggregates can also be demonstrated through a theory named aggregation-induced intersystem crossing (AI-ISC), which was established by Jiang and Zhang [44]. On the basis of theoretical simulations, it was observed that the process of forming aggregates of fluorophores can improve the energy match between excited singlet and triplet states, thereby reducing their energy gap ( $\Delta E_{ST}$ ). Consequently, the yield of the triplet excited state would be improved thanks to the promoted ISC rate, hence boosting ROS generation (**Figure 5**). It seems reasonable that the minimization of excited energy loss through non-radiative decay and AI-ISC synergistically make aggregates of AIEgens well-performing ROS generators. More importantly, considering their significant fluorescence properties, AIEgens are promising as excellent theranostic materials for FLI-guided PDT application.

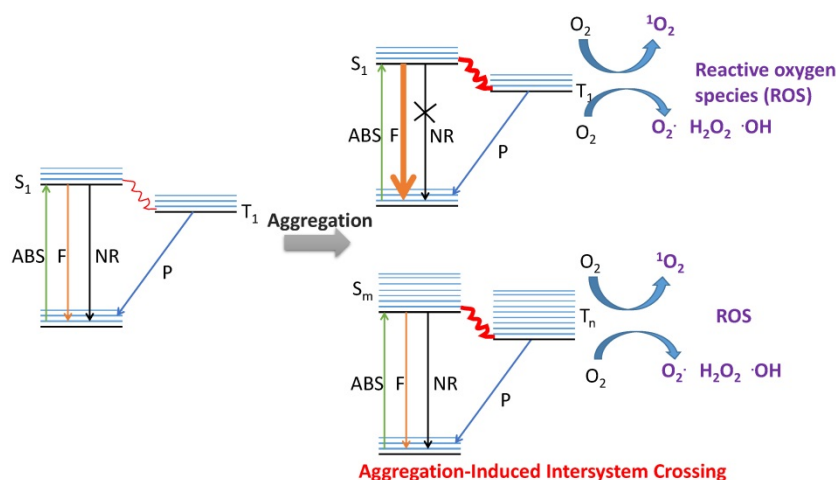


**Figure 5.** Diagrammatic explanation of the advantages of AIEgens in PDT.

Apart from mechanism theories, experimental measurements have also been carried out to verify the much higher ROS generation efficiency of AIE aggregates compared to molecular AIE species [45], as well as to demonstrate the relationship between  $\Delta E_{ST}$  and ROS generation [46]. AIEgens TPDC, TPPDC and PPDC were smartly designed and found to exhibit orderly reduced  $\Delta E_{ST}$  values of 0.48, 0.35 and 0.27 eV, respectively (Figure 6) [46].  $^1O_2$  measurement was carried out using 9,10-anthracenediyl-bis(methylene) dimalonic acid (ABDA) as a  $^1O_2$  indicator, and employing Rose Bengal (RB) as the standard PS. The corresponding  $^1O_2$  quantum yields were measured to be 0.28, 0.32 and 0.89, solidly indicating that enhancing ISC efficiency obtained by the reduction of energy gap between the singlet and triplet excited states can improve  $^1O_2$  generation efficiency. In addition, *in vitro* experiments in HeLa cells showed that these pre-fabricated AIEgens-based NPs can be successfully used in cellular bio-imaging (Figure 6B); Figure 6E-F depict that PPDC, with both the smallest  $\Delta E_{ST}$  and the highest ROS generation efficiency, provided the best performance for cancer cell ablation through the PDT pathway compared to the others [46]. This study revealed that, guided by the established theory, predictable material performance can be achieved through molecular design.

Many other advantages of AIEgens in theranostics have also been witnessed in several

aspects. Firstly, as one of the essential features of materials for bio-applications, good biocompatibility is significantly important. Unlike quantum dots having toxic metal atoms such as cadmium and mercury, AIEgens comprised of organic components usually exhibit good biocompatibility, which facilitates their applications in diagnosis and therapy [21,25]. In addition, the use of AIEgens offers the opportunity to readily fine-tune the chemical and photophysical properties of theranostic platforms by deliberate modulation of the chemical structures of AIEgens and systematic variation of their substitution, because almost all the explored AIEgens are small organic molecules. Moreover, it was noticed that the nano-aggregate size of AIEgens generally ranges from dozens to hundreds of nanometers, which makes AIEgen NPs suitable for specifically accumulating in tumor tissue via the EPR effect. It has been demonstrated that the EPR effect can allow AIEgen NPs to accumulate in tumor tissue over normal tissues via leaky blood vessels surrounding the tumor [47]. Benefiting from the EPR effect, AIEgen NPs are capable of being utilized in specific imaging and therapy towards tumor without the requirement of extra targeting ligands [48]. Additionally, the remarkable fluorescence properties of AIEgens make them extraordinary for FLI, which is the most commonly used imaging modality in theranostics due to the merits of fluorescence technology. Therefore,

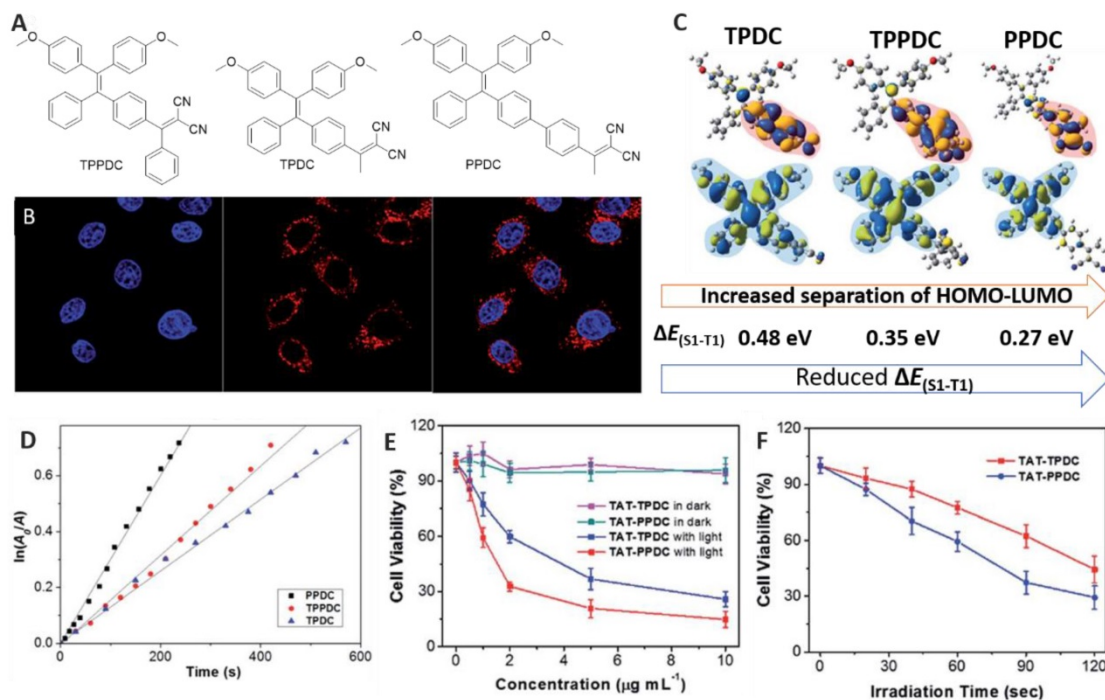


**Figure 6.** (A) Structures of AIEgens. (B) Confocal images of HeLa cells upon incubation with TAT-PPDC NPs. (C) Molecular orbital amplitude plots of HOMO and LUMO energy levels of AIEgens. (D) The decomposition rates of ABDA caused by AIEgens. (E) The viability of cancer cells upon treatment with AIEgens NPs with or without light irradiation. (F) The viability of HeLa cells incubated with TAT-TPDC NPs and TAT-PPDC NPs for different durations of light irradiation. Reproduced with permission from [46], copyright 2015 Royal Society of Chemistry.

FLI-involved theranostics can be facilely constructed through incorporating a therapeutic function. Furthermore, it has been reported that some drugs inherently exhibit AIE characteristics. For example, quercetin, a natural bioflavonoid that acts as an immune system modulator and potent polyphenol antioxidant, has been determined to be AIE-active and powerful for *in vitro* and *in vivo* bioimaging [49]. The AIE features of those drugs enable them to be ideal theranostic candidates.

## Recent development

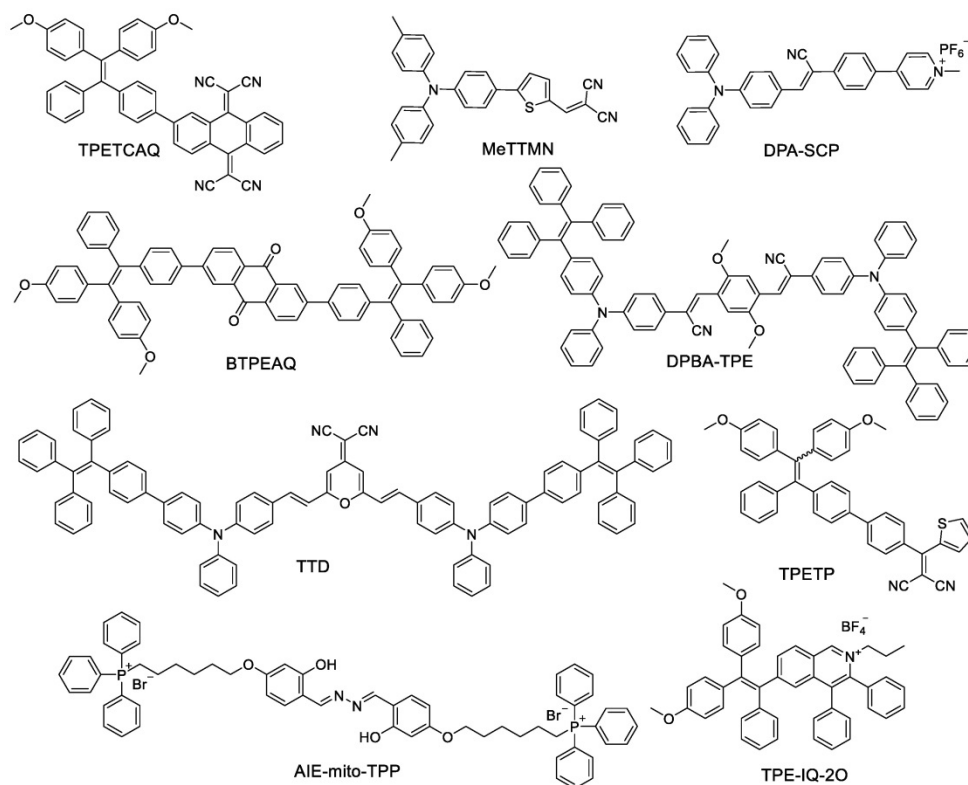
### Fluorescence imaging (FLI)-guided photodynamic therapy (PDT)

Inspired by the high performance of AIEgens in both FLI and PDT, AIEgens have been extensively used in applications of FLI-guided PDT [37]. Some previously reported AIE-active fluorophores/PSs are shown in **Scheme 1**. They generally comprise electron-donor (D) and -acceptor (A) units to construct a conjugated structure with very strong D-A effect, which leads to separation of HOMO and LUMO distributions and decreased singlet-triplet energy gap simultaneously, resulting in high efficiency of ROS generation. Some of these AIEgens (such as AIE-mito-TPP and TPE-IQ-2O) are functionalized with pyridinium or triphenylphosphine, enabling AIEgens to selectively accumulate in

mitochondria, which have been proven to be ideal sub-cellular organelles to deliver PDT.

High specificities of imaging and therapy towards lesions are crucial for FLI-guided PDT applications, because it can maximize therapeutic efficacy and minimize side effects. Targeted delivery of diagnostic and therapeutic agents is a great challenge in cancer treatment, and limited successes in FLI-guided PDT for cancer therapy have been reached by some driving forces, such as enzyme, non-enzyme protein, ROS, glutathione (GSH), slightly acidic microenvironment of tumor tissues, folate, membrane potential difference of mitochondria, and the EPR effect.

Proteins are a family of indispensable bio-macromolecules in living organisms, and their abnormal expression is usually associated with diseases. A series of proteins including Cathepsin B, HAase, MMP-14, MMP-2, NQO1, DT-diaphorase, PTK7, Caspase-3 and TfR, have been found to be expressed by tumor cells and successfully utilized as biomarkers to drive drug delivery and/or to monitor responses to cancer treatment [50]. As a promoter of almost all metabolic processes, enzymes can effectively activate theranostic materials prepared by ingenious design [51]. Cathepsin B, a lysosomal protease overexpressed in many types of cancer cells [52], is able to specifically cleave the -Gly-Phe-Leu-Gly- (GFLG) peptide sequence [53].  $\alpha_v\beta_3$  integrin



**Scheme 1.** Some of the reported AIEgens for FLI-guided PDT.

is another enzyme overexpressed in cancer cells, and it can selectively interact with cyclic arginine-glycine-aspartic acid (cRGD), which endows targeted drug delivery towards cancer cells [54]. Encouraged by these interesting properties of Cathepsin B and  $\alpha_v\beta_3$  integrin, a dual-targeted enzyme-activatable bio-probe was designed and synthesized by Liu and co-workers (Figure 7A) [55]. This bio-probe is comprised of AIE fragment TPECM for both imaging and PDT, Cathepsin B-responsive GFLG peptide,  $\alpha_v\beta_3$ -attachable cRGD group and hydrophilic units. This bio-probe maintained a fluorescence "off" state and low level of ROS generation in aqueous environment, because its good hydrophilicity enabled it to be well dissolved in aqueous solution and the free intramolecular motions

caused excitonic energy consumption. The dual-targeted functionality made the probe selectively accumulate in cancer cells. In addition, *in situ* cleavage of GFLG brought about the release, aggregation and "light up" emergence of TPECM, providing real-time cancer cell imaging with a high signal-to-noise ratio (Figure 7B). Furthermore, ROS production was simultaneously well-performed by the aggregated TPECM in cancer cells, leading to highly selective and efficient ablation of cancer cells [55].

A non-enzymatic protein-activated FLI-guided PDT AIE theranostic system has also been explored by employing transferrin receptor (TfR), a type of transmembrane glycoprotein [56]. TfR is present in both normal and cancer cells, and its expression level increases with cell proliferation rate; thus, its quantity

in cancer cells is much higher than that in normal cells. On the basis of this finding, early diagnosis of cancer could be achieved through quantitative detection of TfR [57,58]. In addition, TfR has also been proven to be an excellent delivery target for therapeutic agents [59]. In 2016, a theranostic bio-probe (TPETH-2T7) was prepared by conjugating a red-emissive AIE moiety to T7 peptide that possessed a remarkable capability to bind with TfR (Figure 8) [60]. Free TPETH-2T7 was barely emissive, but it selectively illuminated TfR-overexpressed cancer cells over normal cells by showing red fluorescence in real time upon specific interaction with TfR, resulting from the restriction of intramolecular motions of TPETH. The high ROS generation efficiency of TPETH enabled effective application for photodynamic ablation of MDA-MB-231 cancer cells with light illumination, and both cell morphology changes and membrane disintegration were observed within a short period of light irradiation. This work exploited an efficient avenue for targeted delivery of theranostic reagents, specific imaging and killing of cancer cells by FLI-guided PDT [60].

Apart from TfR, folate receptor (FR) is another non-enzymatic protein that has been utilized to achieve FR-targeted delivery of various theranostics [61,62], because FR is

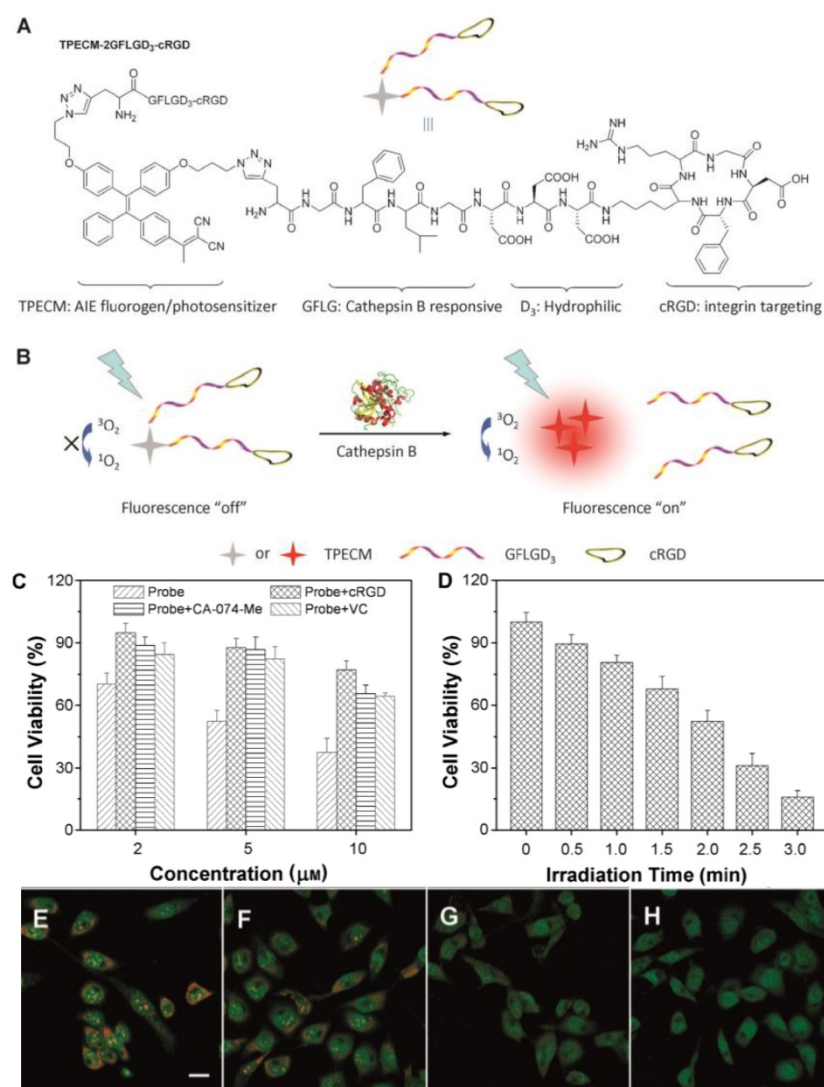


**Figure 7.** Cathepsin B-driven cancer cell FLI diagnosis and PDT. **(A)** The structure of TPECM-2GFLGD<sub>3</sub>-cRGD. **(B)** Schematic illustration of probe activation by Cathepsin B. **(C)** Viability of MDA-MB-231 cells under different conditions. **(D)** Inhibition of MDA-MB-231 cell growth under different conditions. **(E-H)** Observation of lysosomal disruption of MDA-MB-231 cells as induced by the probe upon irradiation with light in the presence of acridine orange as the indicator. The cells were treated with (E) light only, (F) the probe without irradiation, (G) the probe with light irradiation for 1 min, or (H) the probe with light irradiation for 2 min. Reproduced with permission from [55], copyright 2015 Wiley-VCH.

overexpressed in many types of cancer cells and the binding affinity of folate to FR is quite high [63]. A bio-probe was assembled by decorating red-emissive AIE dots (DPBA dots) with both folate and triphenylphosphine (Figure 9) [64]. The former was employed to selectively internalize into FR-positive cancer cells; the latter endowed the probe with selective accumulation in mitochondria, which has been proven to be an ideal subcellular organelle to deliver PDT. By applying the dual-targeted strategy, AIE dots specifically illuminated the mitochondria of cancer cells, and produced abundant ROS *in situ* that lead to mitochondrial dysfunction and consequently triggered cell apoptosis and death (Figure 9). This strategy thus opened up new opportunities to explore theranostic agents for accurate delivery and efficient therapy [64].

It is known that excessive ROS can trigger cell apoptosis or cell death by deregulation of protein

functions and/or oxidative modification of cellular macromolecules [43]. Actually, a low balanced level of ROS under normal physiology is essential for various biological processes including cell homeostasis, proliferation, signaling and aging. In addition, as a result of some factors including mitochondrial malfunction, oncogenic stimulation and increased metabolic activity, cancer cells have higher levels of ROS than normal cells [65]. The difference in ROS levels favors the development of tumor-targeted imaging and therapy. On the other hand, some chemical units, such as aminoacrylate (AA), can be cleaved by ROS, further providing stimulated responses such as turn-on fluorescence, which could be used to achieve diagnostic imaging of cancer cells. For example, a theranostic compound (named TPETP-AA-Rho-cRGD) containing red-emissive AIE-active unit,  $^1\text{O}_2$ -cleavable linker AA, green-emissive  $^1\text{O}_2$ -responsive rhodol fragment and cRGD, was successfully constructed (Figure 10) [66]. The existence of TPETP endowed the compound with red emission in aqueous solution; thus, it possesses a self-tracking function. With the assistance of cRGD, TPETP-AA-Rho-cRGD specifically targeted  $\alpha_v\beta_3$ -overexpressing cancer cells. Furthermore, ROS that was efficiently produced by TPETP upon light irradiation rapidly reduced DA-MB-231 cell viability, and a half-maximal inhibitory concentration ( $\text{IC}_{50}$ ) of 8.3  $\mu\text{M}$  was determined. In comparison, the  $\text{IC}_{50}$  of the probe was 219.1  $\mu\text{M}$  in dark conditions. The high ratio of  $\text{IC}_{50}$  values in the dark and upon light irradiation indicated its great potential as an excellent therapeutic agent. More importantly, by exploiting this theranostic platform, real-time *in situ* monitoring of ROS production during PDT application of cancer cells was smoothly accomplished [66].

The tripeptide glutathione (GSH) is another driving force for conducting diagnostic imaging of cancer cells. GSH is a critical biomolecule in a variety of cellular processes including cell metabolism, antioxidant defense, cell differentiation, as well as balancing detoxification and antioxidation of

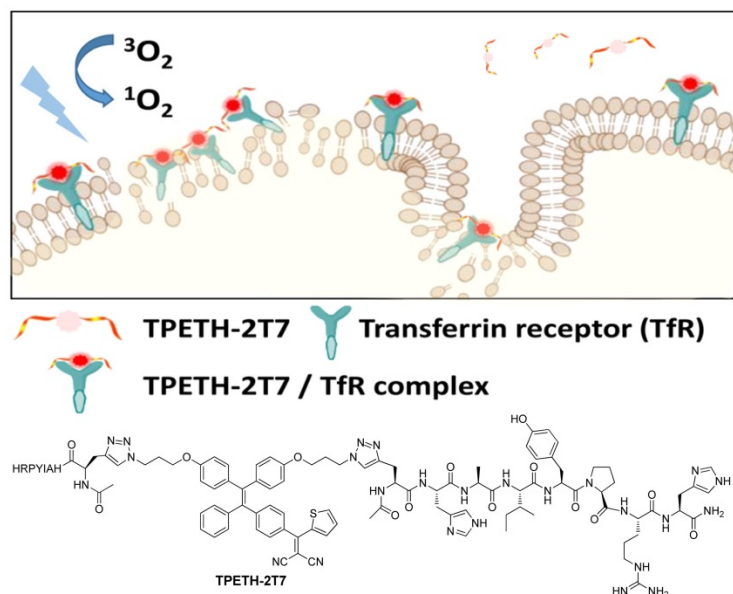


**Figure 8.** Tfr-driven FLI-guided PDT. Reproduced with permission from [60], copyright 2016 American Chemical Society.

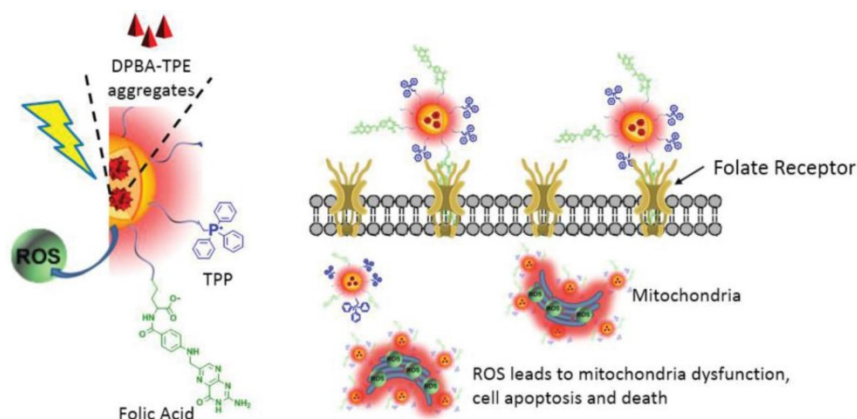


**Figure 9.** Cellular and mitochondrial dual-targeted AIE organic dots for FLI-guided PDT. Reproduced with permission from [64], copyright 2015 WILEY-VCH.

many cellular functions [67]. It has been demonstrated that GSH is overexpressed in many cancer cells over normal cells [68]. As disulfide bond is responsive to GSH, it has been employed as a linker between AIEgens and cancer cell-targeting agents. A novel bio-probe was proposed in this way, in which the disulfide bond can be cleaved by intracellular GSH of cancer cells. Meanwhile, the released AIEgens aggregated and illuminated cancer cells, achieving real-time monitoring of PS activation. In addition, the generation of ROS by AIEgens was remarkably promoted by light illumination, and targeted cancer cell ablation was realized [69]. Later on, Liu's group [70] reported a bio-probe TPETF-NQ-cRGD composed of a red-emissive chromophore PS (TPETF) with AIE

characteristics, cRGD tripeptide for targeting cancer cells and the fluorescence quencher moiety 2,4-dinitrobenzenesulfonyl chloride (NQ) (Figure 11A). The probe was originally non-emissive in the physiological pH range. After the probe simultaneously targeted cRGD-GSH dual-overexpressed cancer cells and was *in situ* treated with GSH, bright fluorescence emerged and remained constant, owing to the elimination of NQ quencher by GSH. Moreover, the authors demonstrated that cancer cells could be completely ablated when 32  $\mu\text{M}$  of the probe was irradiated with white light for 3 min at a power density of 0.25  $\text{W}/\text{cm}^2$ . In this work, both recognition and ablation of cancer cells were achieved by using the dual-targeted bio-probe [70].

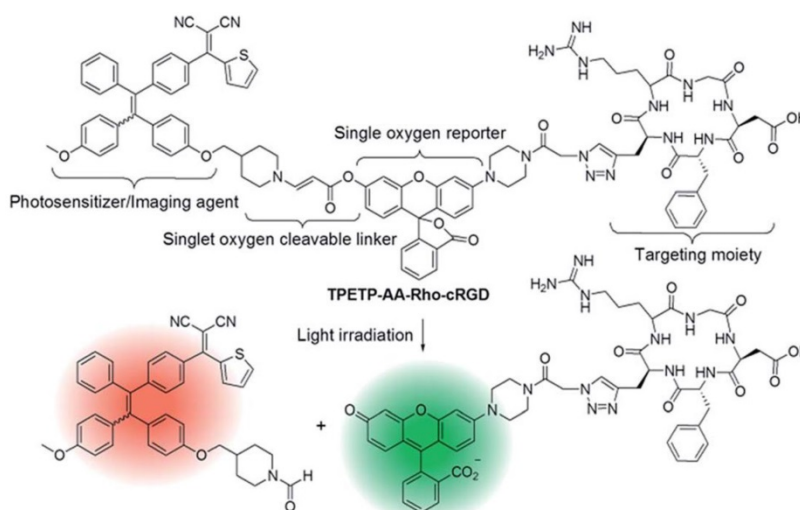


Figure 10. ROS-driven FLI-guided PDT. Reproduced with permission from [66], copyright 2016 Royal Society of Chemistry.

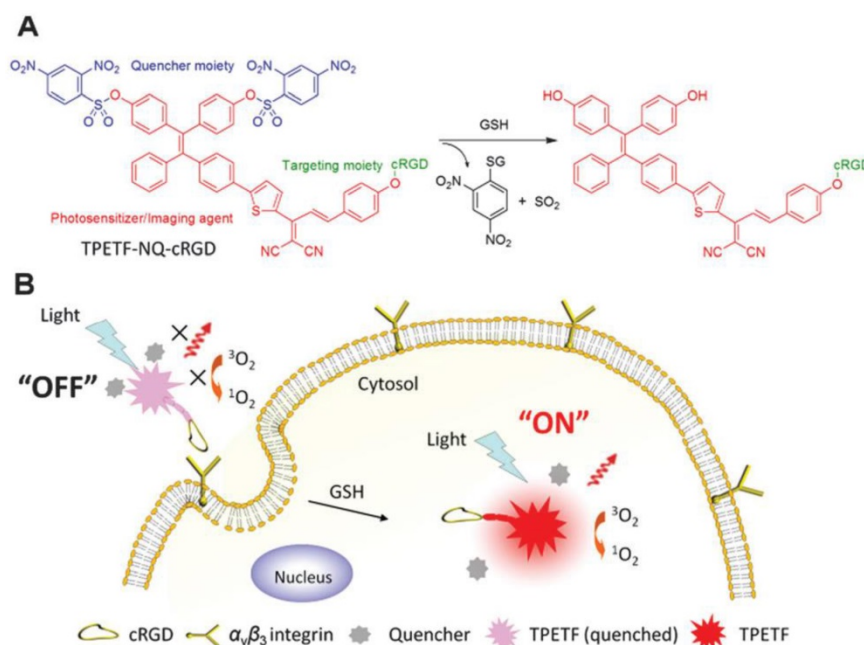
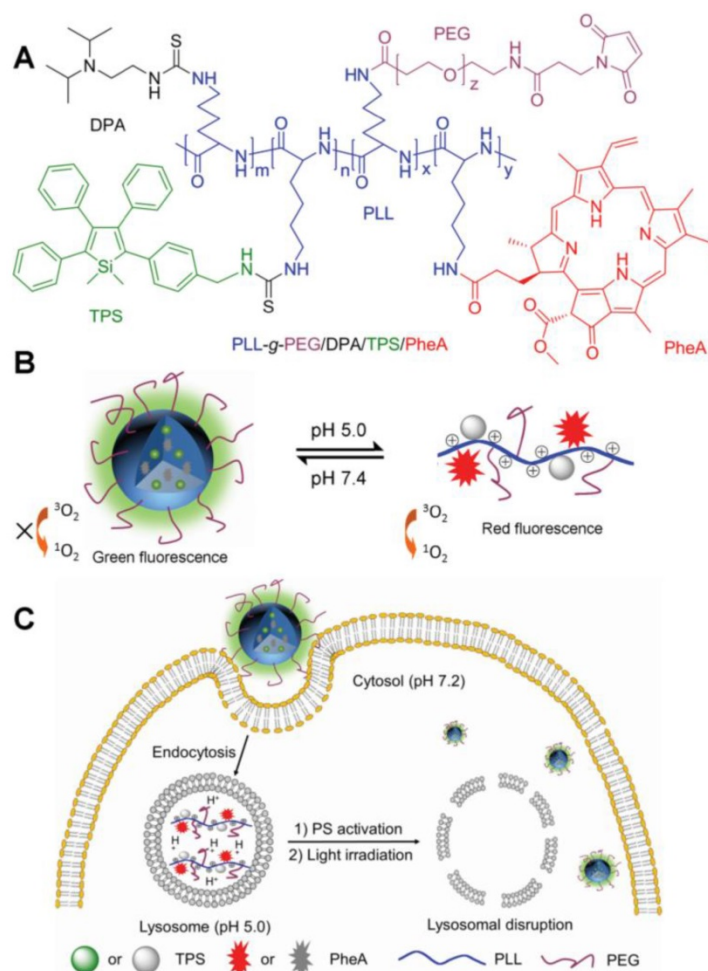


Figure 11. GSH-driven FLI-guided PDT. Reproduced with permission from [70], copyright 2016, Royal Society of Chemistry.

Tumor tissues have lower extracellular pH values (6.5 to 6.9) than normal tissues, presenting a slightly acidic nature [71]. This phenomenon is attributed to the excess accumulation of lactic acid in extracellular milieu resulting from the more active glycolysis and proton-pump activities on plasma membranes of cancer cells than that of normal cells [72,73]. It has been speculated that the slightly acidic nature of tumor tissues could be useful for the development of cancer theranostic materials that are designed to have enhanced imaging signals and therapeutic activities under slightly acidic conditions compared with neutral conditions. Obviously, the development of pH-responsive theranostics that are activatable in the pH range of 6.5 to 6.9, is a great challenge. Additionally, lysosome is an important cellular organelle that features a weakly acidic environment (pH 4.5-5.0), which is commonly used as a target for pH-responsive cancer diagnosis. As illustrated in **Figure 12**, an AIEgen-involved pH-activatable probe that can provide a fluorescence

change upon uptake by cancer cells and entrapment in lysosomes was developed [74]. The probe (PLL-g-PEG/DPA/TPS/PheA) was mainly composed of an AIE fluorophore (TPS), an ACQ PS pheophorbide (PheA), a pH-responsive diisopropylamino (DPA), and cRGD tripeptide for targeting cancer cells with overexpressed  $\alpha_v\beta_3$  integrin. At physiological conditions (pH 7.4), NPs of this probe were formed that emit green fluorescence from TPS fragments. Upon uptake by cancer cells, these NPs were selectively entrapped in lysosomes; then, the acidic environment promoted protonation of DPA, making the NPs disassemble. Consequently, the probe in single molecular state showed red fluorescence of PheA, and the produced ROS led to disruption of the lysosomal membrane and cell apoptosis. Interestingly, the green fluorescence of TPS could be restored following leakage of the probe from lysosomes to cytoplasm, which has a pH value of 7.2. This probe design thus represents an advanced strategy for achieving therapeutic response [74].



**Figure 12.** Slight acid-driven FLI-guided PDT. **(A)** Chemical structure of PLL-g-PEG/DPA/TPS/PheA. **(B)** Schematic illustration of the pH-activatable probe. **(C)** Schematic representation of the probe used for self-tracking, cancer cell imaging, phototoxicity restoration in the acidic lysosome, and *in situ* monitoring of lysosomal membrane disruption as an indicator of therapeutic response and cell death prediction. Reproduced with permission from [74], copyright 2015 Wiley-VCH.

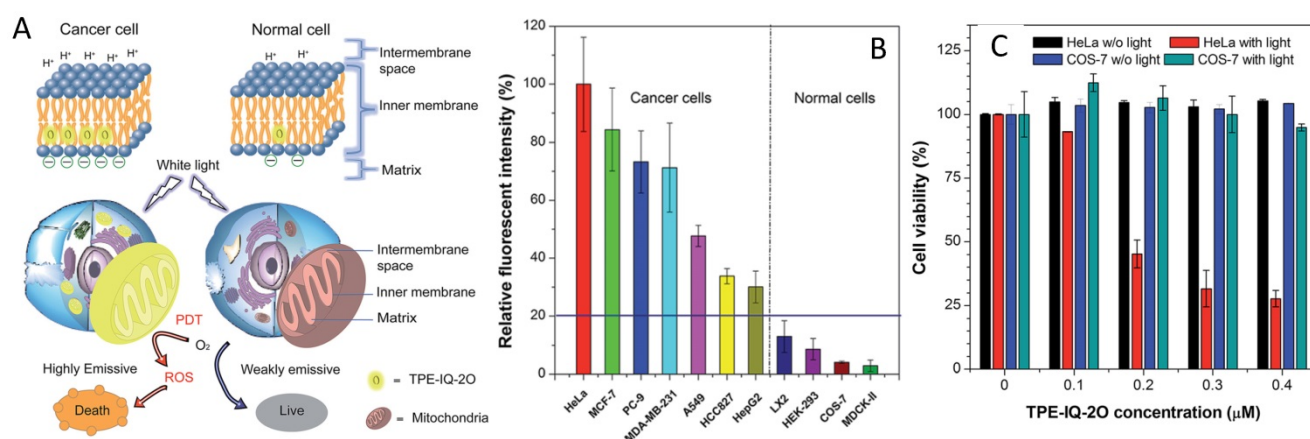


**Figure 13.** Difference of mitochondrial membrane potential-driven FLI-guided PDT. **(A)** Schematic illustration of selective mitochondrion imaging in cancer cells and a PS for PDT. **(B)** Relative fluorescence intensity of different cells incubated with TPE-IQ-2O. **(C)** Cell viability of HeLa cells and COS-7 cells stained with different concentrations of TPE-IQ-2O in the absence or presence of white light irradiation. Reproduced with permission from [77], copyright 2017 Royal Society of Chemistry.

It has been verified that the mitochondrial membrane potential of cancer cells is higher than that of normal cells, and such difference can be utilized for cancer cells discrimination and selective therapy (Figure 13A). Some AIEgens containing positive charges, such as AIE-mito-TPP and TPE-IQ-2O (Scheme 1), were prepared and employed as imaging agents for selectively staining cancer cell mitochondria [75-77]. Tang's group [77] prepared the AIE-active TPE-IQ-2O, which is positively charged and comprised of pyridinium and a TPE unit. TPE-IQ-2O did not emit light in culture medium, but it was able to selectively accumulate in and light up mitochondria in cancer cells over normal cells, mainly owing to the difference in mitochondrial membrane potential (Figure 13B). In addition, the high capability of TPE-IQ-2O for ROS generation enabled it to be a remarkable therapeutic agent for PDT application. More importantly, selective killing of cancer cells was realized, benefiting from its specific accumulation in cancer cells (Figure 13C) [77]. This presented system needs neither any additional targeting group nor PS, thus representing a simply fabricated and significantly useful theranostic system for cancer diagnosis imaging and therapy.

The EPR effect, which allows macromolecules and nanomaterials to accumulate in tumor tissue over normal tissues via leaky blood vessels surrounding the tumor, is one of the most extensively used driving forces for targeted imaging and therapy [47,78]. Some AIE dots have been recently prepared and utilized in FLI-PDT applications for cancer treatment that involve the EPR effect for targeted delivery [48,79]. Liu and co-workers [48] synthesized an NIR-emissive AIEgen (named TPETCAQ, and the structure is shown in Scheme 1) with relatively long-wavelength absorption. TPETCAQ NPs were fabricated through a nanoprecipitation strategy with assistance from

amphiphilic copolymer 1,2-distearoyl-sn-glycero-3-phosphoethanolamine-*N*-[methoxy (polyethylene glycol)] (DSPE-PEG) as the encapsulation matrix. In addition, aiming to improve the cellular internalization efficiency, a cell membrane penetration peptide (RKKRRQRRC) was grafted on the surface of TPETCAQ NPs. The assembled TPETCAQ NPs stained 4T1-luc cancer cells, and specifically illuminated tumor tissue of mice via the EPR effect (Figure 14 A, D). Moreover, TPETCAQ NPs were determined to be an excellent PS for ROS generation with even surprisingly higher efficiency than Ce6, which is one of the most efficient PSs reported so far. *In vivo* experiments revealed that the cytotoxicity of TPETCAQ NPs was negligible under dark conditions, while the cell viability remarkably decreased upon light irradiation (Figure 14B). *In vivo* antitumor evaluation of TPETCAQ NPs on 4T1-luc tumor-bearing mice showed that TPETCAQ NPs were able to significantly reduce tumor size, indicating their high therapeutic efficacy for PDT [48]. These exciting results created new opportunities for the development of clinical PDT.

In the field of FLI-guided therapy, one of the urgent challenges facing scientists now is how to overcome the low penetration depth of light in biological tissue. In this context, two-photon PDT (TP-PDT) has recently emerged on the basis of the rapid expansion of two-photon imaging, and has displayed great potential for practical applications [80]. It has been demonstrated that TP-PDT successfully achieves treatment of deeper tumors and tiny pathologic regions with minimal photo-damage to the surrounding normal tissue, benefiting from the higher penetration depth and better spatial selectivity [80,81]. In 2017, the groups of Liu and Qian [82,83] reported two AIE theranostic systems for FLI-guided TP-PDT. As depicted in Figure 15, cell membrane

penetrating peptide-modified AIE dots (T-TPEDC dots) were readily fabricated [83]. Their two-photon absorption (TPA) cross section was 3500 GM at 850 nm, which was extremely large compared to other two-photon materials, offering great potential for TP-PDT. In order to assess the TP-PDT efficacy of T-TPEDC dots, the populations of viable and necrotic cells were measured by Calcein-AM/propidium iodide (PI) double staining. It was found that HeLa cells outside the scanned areas exhibited green fluorescence from Calcein-AM, suggesting good biocompatibility and negligible cytotoxicity of T-TPEDC dots under dark conditions. With the increase of scan numbers in the scanned area, the population of PI-positive necrotic cells generally increased (Figure 15C-E). Furthermore, selective *in vivo* closure of brain blood vessels was performed *in vivo* using TP-PDT. The results showed that two-photon light irradiation enabled the scanned area to exhibit very weak fluorescence, while the fluorescence intensity of surrounding blood vessels was constant throughout the irradiation (Figure

15F-G), indicating the high spatial selectivity and efficient ROS generation of the TP-PDT strategy for *in vivo* experiments [83].

In summary, a series of AIEgen-based theranostic materials have been explored for FLI-guided PDT. These materials generally possess bright fluorescence emission, high photostability, good chemical stability, excellent targeted accumulation in cancer cells or tumor tissue with the aid of specific targeting components, great therapeutic efficacy especially for *in vitro* evaluation thanks to their remarkable ROS generation efficiency, as well as high spatial selectivity of therapy resulting from the use of TP-PDT. Absolutely, other conceptually new approaches to design AIEgens for FLI-guided PDT applications will be devised shortly. However, since AIEgens are newly explored materials in the field of theranostics, the utilization of AIE-involved PDT is still at a very early stage. Considering the unclear safety level of AIEgens in humans, further clinical use of AIE PS will be a long-term goal requiring great efforts.

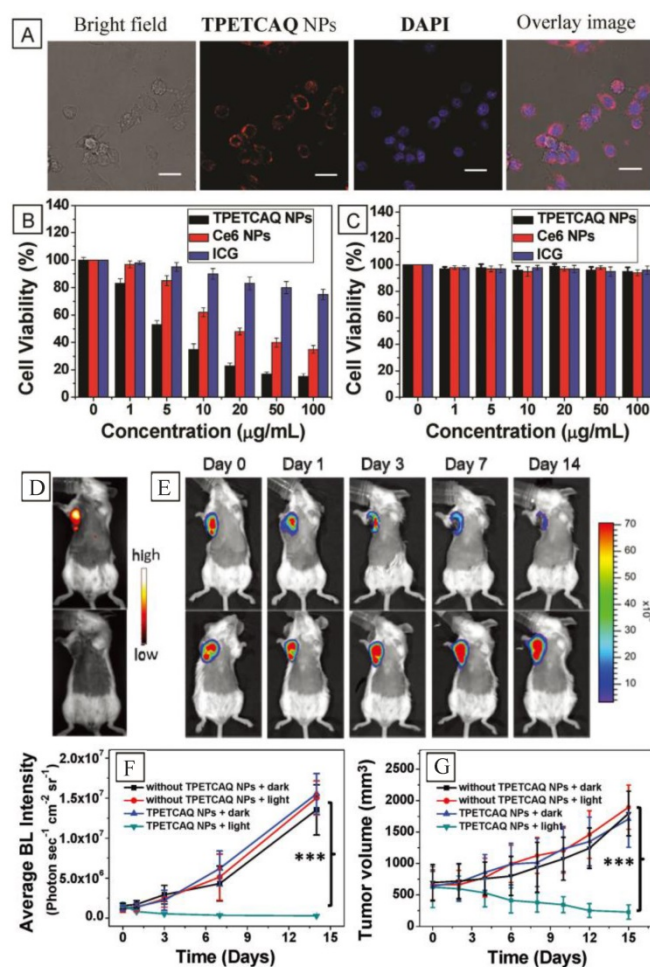


**Figure 14.** A highly efficient, photostable PS and NIR-emissive AIEgen for image-guided photodynamic anticancer therapy. (A) Confocal images of 4T1-luc cancer cells after incubation with TPETCAQ NPs. Cell viability of different PS-treated 4T1-luc cancer cells (B) under light irradiation (60 mW/cm<sup>2</sup>, 5 min) or (C) in the dark. (D) Fluorescence imaging of 4T1-luc tumor-bearing mice after intratumoral administration of TPETACQ NPs (top) or saline (bottom) at 1 h postinjection. (E) Quantitative analysis of bioluminescence signals of 4T1-luc tumor in different mice groups. (F) Tumor volume measurement for different groups of mice. Reproduced with permission from [48], copyright 2017 Wiley-VCH.

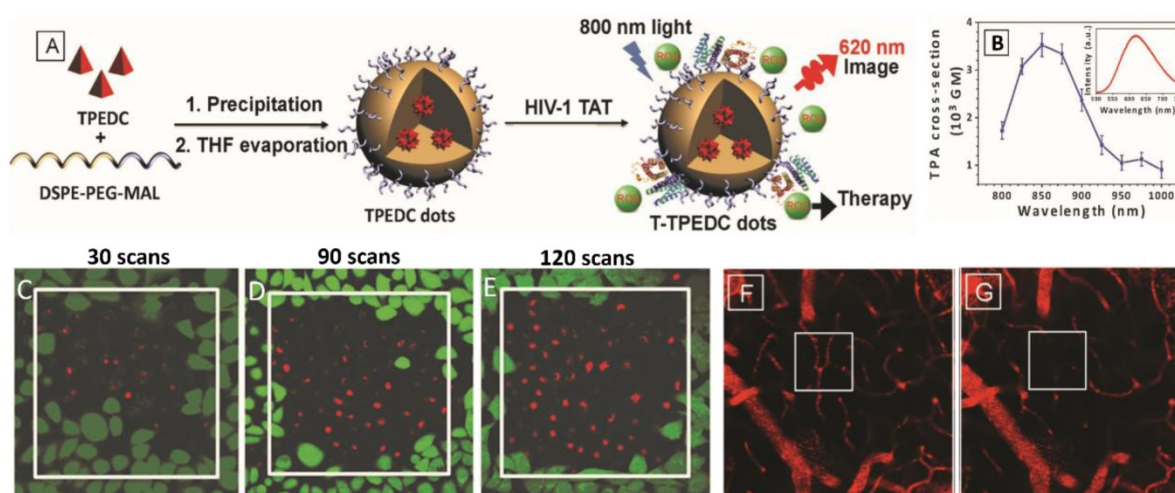


**Figure 15.** The use of AIEgens in TP-PDT. **(A)** The preparation of T-TPEDC dots. **(B)** Two-photon absorption cross section of T-TPEDC dots at different wavelengths. HeLa cells incubated with T-TPEDC dots were irradiated for different two-photon scans: **(C)** 30 scans, **(D)** 90 scans, and **(E)** 120 scans. **(F-G)** Pre-irradiation (F) and post-irradiation (G) images of brain blood vessels of a mouse treated with T-TPEDC dots (8 mg/kg based on TPEDC) and two-photon excitation. Reproduced with permission from [83], copyright 2017 Wiley-VCH.

### Chemiluminescence imaging (CLI)-guided chemiexcited PDT

Unlike fluorescence that refers to light emission of a substance by the absorption of light or other electromagnetic radiation, chemiluminescence is light emission without the requirement of an external excitation source. As the result of energy release from a chemical reaction, chemiluminescence is usually conducted by employing a high-energy compound and  $\text{H}_2\text{O}_2$  as reagents. The electronic excited state of chemiluminescence is the product of a chemical reaction rather than that of the absorption of a photon. Compared with traditional fluorescence imaging, chemiluminescence imaging holds distinct advantages such as *in situ* activation, deeper tissue penetration, higher signal-to-noise ratio and avoidance of damage caused by an external excitation source, making it a promising tool for *in vivo* diagnosis [84,85]. Moreover, chemiluminescence has been demonstrated to be an appropriate candidate for specific tumor imaging because the amount of  $\text{H}_2\text{O}_2$  inside solid tumors is generally higher than that inside normal tissue [86].

In 2017, Liu's group [87] reported the first example of *in vivo* CLI-guided chemiexcited PDT by using AIEgens as the PS. In this work, C-TBD NPs were prepared by co-encapsulation of F-127, soybean oil, AIEgen TBD, and bis [2,4,5-trichloro-6-(pentylloxycarbonyl) phenyl] oxalate (CPPO) (Figure 16A). Each component played an indispensable role in CLI-guided chemiexcited PDT, especially TBD and CPPO: TBD was selected as the PS considering its long-wavelength emission and great capability for ROS production; CPPO was used to react with  $\text{H}_2\text{O}_2$ , yielding the high-energy 1,2-dioxetanedione

intermediate, which was the species for exciting TBD through a chemically initiated electron exchange luminescence (CIEEL) process, finally generating both luminescence and  $^1\text{O}_2$  without any light source. The results of *in vivo* experiments revealed that C-TBD NPs can selectively illuminate tumors in mice through chemiluminescence imaging, resulting from the high  $\text{H}_2\text{O}_2$  amount inside tumors. In contrast, by means of FLI, fluorescence signals were observed in both tumor and mononuclear phagocyte system organs (such as the liver) (Figure 16B-C). It was described that the ROS generated via the chemiexcitation process can moderately inhibit the growth of tumor. Furthermore, the addition of  $\beta$ -phenylethyl isothiocyanate (FEITC) was demonstrated to be able to enhance both chemiluminescence signals of the tumor and anti-tumor efficacy as a result of elevated  $\text{H}_2\text{O}_2$  production at the tumor site; in particular, the enhancement of anti-tumor efficacy was remarkably obvious (Figure 16D) [87]. This contribution provided a novel strategy for nanomaterials in cancer imaging and accurate non-invasive tumor therapy by using AIEgens, representing one of the breakthroughs in the area of AIE-based theranostics. On the other hand, it was noticed that the low persistence of chemiluminescence signal compared with FLI could be an issue hampering the practical application of CLI-guided chemiexcited PDT, driving scientists to contribute more efforts to this interesting field.

### FLI-guided chemotherapy (CHT)

As an extensively used clinical method for cancer treatment, CHT is usually performed by interfering with biological processes including DNA replication, transcription and cell division, through many small chemical compounds such as doxorubicin

(DOX), camptothecin (CPT), paclitaxel, S-crizotinib, gemcitabine, 7-ethyl-10-hydroxycamptothecin (SN-38) and etoposide. The key to developing contemporary CHT-based theranostic systems is exploiting extraordinary drug delivery systems, aiming to achieve specific delivery of drugs for both enhancing therapeutic effects and evading side effects [88-92], drug distribution monitoring, drug activation monitoring, and therapeutic response monitoring [93,94].

Encouraged by the great properties of AIEgens in FLI, some AIE-based theranostic platforms have been utilized in the area of FLI-guided CHT in the past few years. These platforms can be divided into three types: therapeutic agents along with AIE features, drugs connected with AIEgens by chemical bonds, and drugs encapsulated in AIEgens. The AIEgens could be pure organic compounds, metal complexes or metal nanoclusters.

In 2016, Tang's group [95] developed a novel therapeutic agent having AIE features. This therapeutic agent (TPE-TMX; **Figure 17A**) was designed on the basis of tamoxifen (TMX), which is a clinically used drug for breast cancer treatment that modulates estrogen receptor (ER) [96]. Replacement of an ethyl group by a phenyl ring enabled TPE-TMX to exhibit AIE features, which made it suitable for cell imaging. In such a way, cellular-level distribution and functions of TMX could be readily monitored. Unmodified TMX was invisible in cells in comparison (**Figure 17B**). Cell imaging experiments revealed that TPE-TMX could specifically target lysosomes of breast MCF-7 cancer cells, showing bright blue emission. Remarkably, the therapeutic efficacy of TPE-TMX was comparative to that of TMX. In addition, TPE-TMX

exclusively inhibited the cell viability of MCF-7 cancer cells instead of other cell lines including HeLa, ER-negative MDA-MB-23, and Cos-7 cells (**Figure 17E-F**). The outstanding performance of TPE-TMX enabled it to be a promising theranostic agent for FLI-guided CHT in breast cancer treatment. The results presented in this work will guide the development of AIE-active drugs, thus establishing insights into pharmacodynamics, as well as realizing distribution monitoring [95].

Apart from drugs with AIE features, various theranostic molecules (as shown in **Scheme 2**) that are composed of an AIE unit, targeting moiety and drug/prodrug, have been prepared and applied in FLI-guided CHT [96-100]. The applied drugs include DOX, chlorambucil, cisplatin and gemcitabine. In some reported systems, responsive and activatable fragments were also conjugated. Moreover, it has been demonstrated that the use of prodrugs is one of the effective tools to realize maximal drug safety. These prodrugs are inactive before targeting to lesions, and their pharmaceutical activities can be restored after contacting lesions. As depicted in **Figure 18**, The pre-synthesized theranostic compound PyTPE-Pt-D5-cRGD contains four fragments: an AIEgen, Pt(IV) prodrug of the anticancer drug cisplatin [99], a hydrophilic unit and cRGD. It was observed that PyTPE-Pt-D5-cRGD was non-emissive and highly stable under exposure to cellular proteins, and it exhibited great capability for specific targeting to  $\alpha_v\beta_3$ -overexpressing cancer cells with the assistance of cRGD. After staining cancer cells, Pt(IV) prodrug was gradually reduced by ascorbic acid to yield the active Pt(II) drug and released the AIE unit PyTPE, which formed aggregates and emitted light in cells.

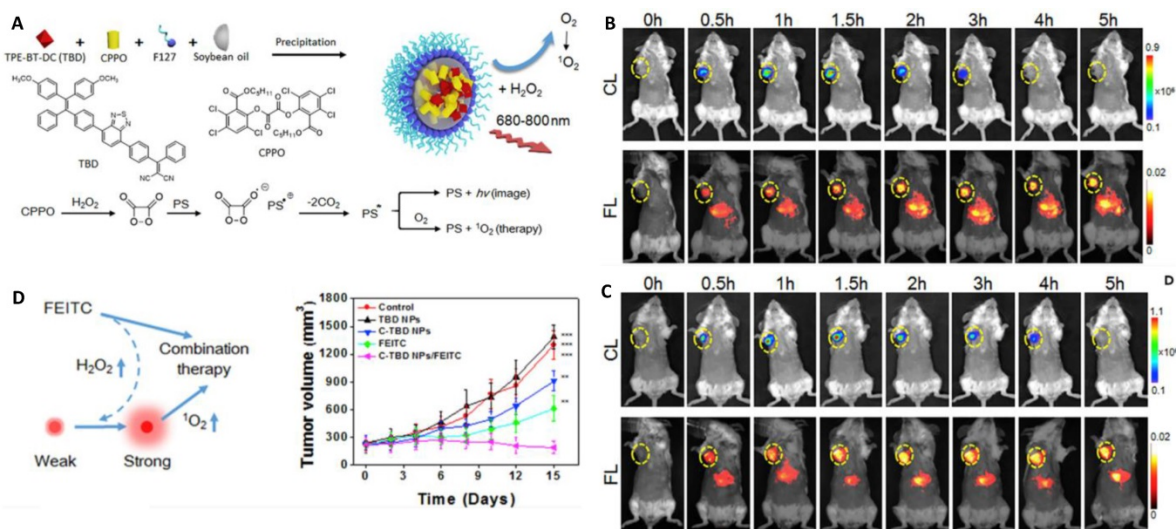


**Figure 16.** Chemiluminescence-guided cancer therapy using a chemiexcited PS. **(A)** The preparation of C-TBD NPs, and illustration of the principle for chemiluminescence and  $^1O_2$  generation of C-TBD NPs in the presence of  $H_2O_2$ . **(B)** Time-dependent *in vivo* chemiluminescence (top) and fluorescence (bottom) images of mice receiving C-TBD NPs. **(C)** Time-dependent *in vivo* chemiluminescence (upper row) and fluorescence (lower row) images of mice successively receiving FEITC and C-TBD NPs. **(D)** Schematic illustration of a hypothetical mechanism of C-TBD NPs and FEITC combination therapy (left), and Tumor growth curves with different therapies (right). Reproduced with permission from [87], copyright 2017 Elsevier.

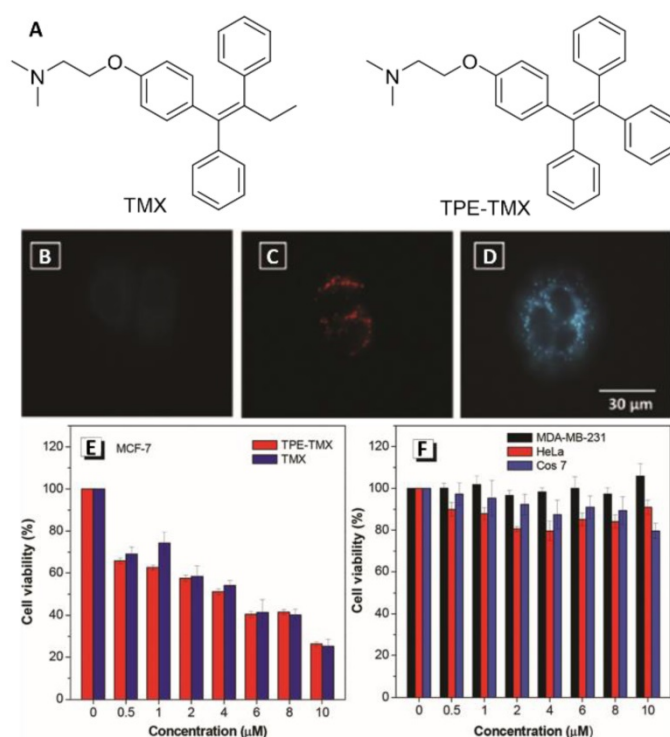
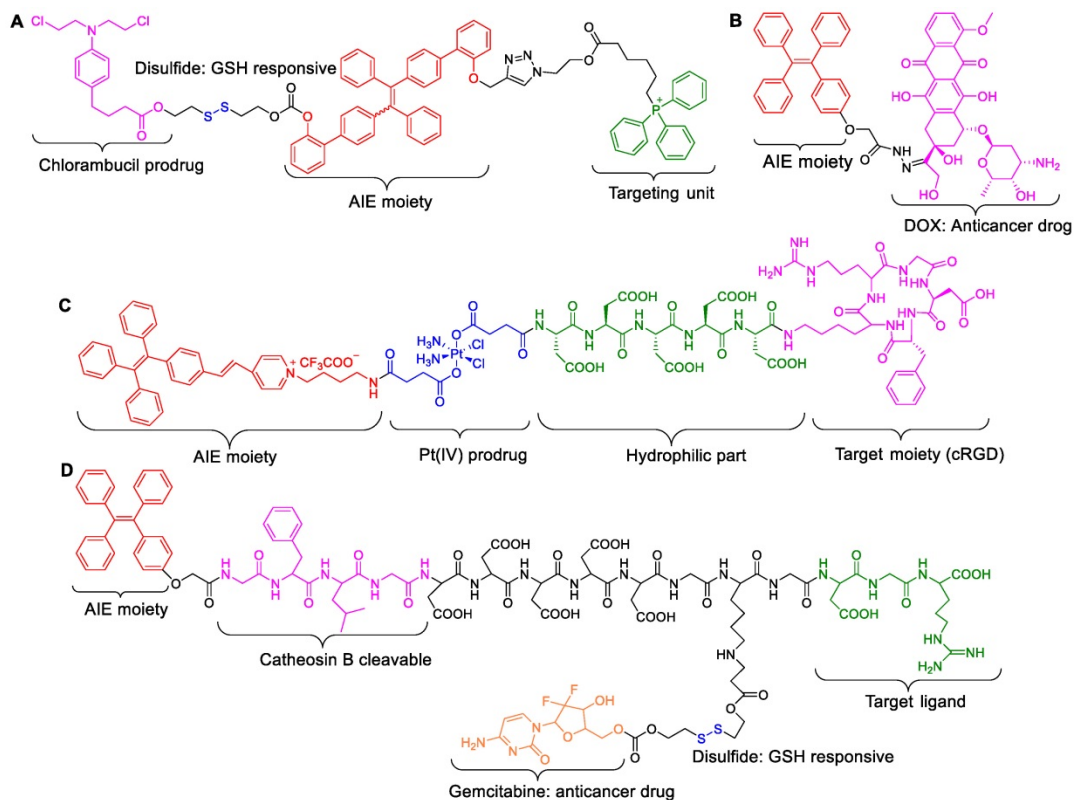


**Figure 17.** A highly fluorescent AIE-active theranostic agent with anti-tumor activity to specific cancer cells. **(A)** Structures of TMX and TPE-TMX. Fluorescence images of MCF-7 breast cancer cells treated with **(B)** TMX, **(C)** a mixture of TMX and LysoTracker Red DND-99 (LTR), and **(D)** TPE-TMX. **(E)** Cell viability of MCF-7 cells incubated with different concentrations of TPE-TMX and TMX. **(F)** Cell viability of different cells in the presence of TPE-TMX at different concentrations. Reproduced with permission from [95], copyright 2016 Royal Society of Chemistry.



**Scheme 2.** AIE-active drugs arranged by AIE moiety, drug and target fragment.

Through this fluorescence turn-on process, intracellular prodrug reduction can be easily monitored. Cytotoxicity evaluation revealed that

PyTPE-Pt-D5-cRGD could efficiently cause cancer cell ablation with a low  $IC_{50}$  of 30.2  $\mu$ M. In contrast, the counterparts of PyTPE-Pt-D5

and PyTPE-C6-D5-cRGD) did not show obvious cytotoxicity towards cancer cells, due to the respective absence of targeting unit and prodrug (Figure 18E). In this work, the light-up nature of AIEgen with aggregation was smartly used for monitoring the prodrug activation processes [98]. In another report, the group of Stang [101] designed and prepared an AIE-active supramolecular metallacage on the basis of their previous contributions [102,103], and successfully utilized it as a theranostic molecule for cancer diagnosis and therapy. The TPE-contained metallacage was assembled by multicomponent coordination, then was encapsulated into NPs by

using both DSPE-PEG and biotin-PEG-DSPE as polymer matrixes (Figure 19). *In vitro* and *in vivo* experiments showed that the obtained NPs selectively targeted biotin receptor-overexpressing cancer cells via receptor-mediated endocytosis, and they specifically accumulated in tumor tissue over normal tissues and selectively illuminated tumors of nude mice bearing HeLa cancer, because of the EPR effect. In addition, these NPs significantly inhibited tumor growth, and their therapeutic efficacy was even higher than commonly used Pt(II) anticancer drugs such as oxaliplatin, carboplatin, and cisplatin [101].

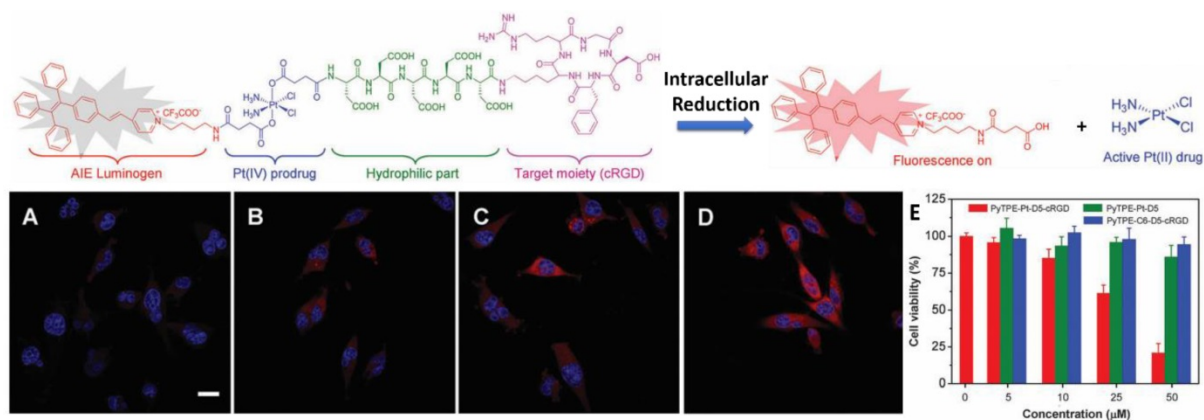


**Figure 18.** (Top) Schematic illustration of the prodrug PyTPE-Pt-D5-cRGD design strategy and the fluorescence turn-on monitoring of drug activation. Confocal images of MDA-MB-231 cells after incubation with PyTPE-Pt-D5-cRGD for 1 h (A), 2 h (B), 4 h (C), and 6 h (D). (E) Cell viability of MDA-MB-231 cells upon treatment with PyTPE-Pt-D5-cRGD at different concentrations. Reproduced with permission from [99], copyright 2014 Royal Society of Chemistry.

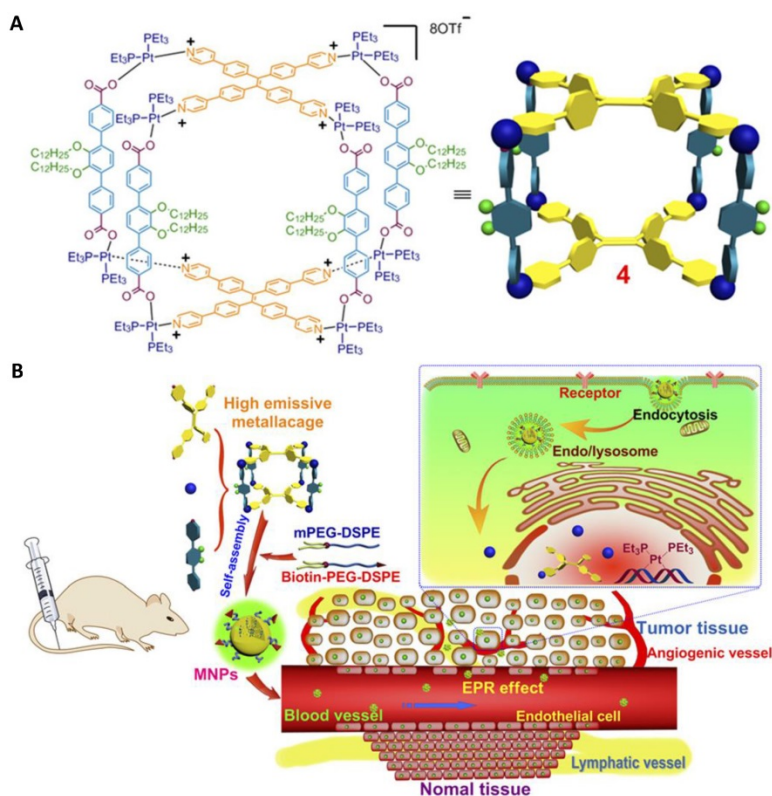


**Figure 19.** TPE-based highly emissive metallacage as a component of theranostic supramolecular NPs. (A) Chemical structure of a tetragonal prism. (B) Scheme of MNPs transportation within blood vessels and accumulation in tumor tissue, followed by receptor-mediated endocytosis. Reproduced with permission from [101], copyright 2016 United States National Academy of Sciences.

Some AIE-active amphiphilic polymers have been prepared and applied as matrixes to encapsulate drugs, yielding corresponding materials for nanotheranostics. As shown in **Figure 20**, polymers TPE-mPEG, TPE-hydrazone-mTPE and Dextran-hydrazone-TPE were synthesized by Wang et al. [104-107], who demonstrated that these polymers were able to self-assemble into micelles, with the encapsulation of DOX providing blue-emissive NPs. Cellular experiments revealed that these formed NPs located in endo/lysosomes of cells after cellular uptake; in addition, the encapsulated DOX was released from these NPs in endo/lysosomes due to the acidic microenvironment. Meanwhile, the fluorescence of TPE was boosted in acidic endo/lysosomes because of termination of the energy transfer between TPE and DOX resulting from the cleavage of the hydrazone bond. Importantly, the drug-loaded NPs displayed dose-dependent cytotoxicity to cancer cells. It has been reported that an AIE-active amphiphilic polymer having both efficient ROS generation capability and ROS-cleavable thioketal linker can be utilized to encapsulate DOX, forming emissive NPs (AIE-NPs/DOX) with light-responsive property [108]. Delivery of DOX could be clearly monitored, and the results revealed that DOX was initially trapped by endo/lysosome trapping and subsequently released to the cell cytoplasm. Moreover, with white light illumination, the generated ROS caused endo-lysosomal membrane rupture and NPs decomposition, both of which promoted the DOX release process, and remarkably

improved intracellular DOX accumulation and retention in cells. The  $IC_{50}$  of AIE-NPs/DOX was 12% of that of free DOX in dark condition and 32% under white light irradiation, indicating the significantly enhanced therapeutic effect caused by light illumination. This exemplary light-controllable drug release would provide a useful strategy to overcome the issue of drug resistance of cancer cells [108].

Apart from AIE-active amphiphilic polymers, some Au nanoclusters have been demonstrated to be AIE-active and have emerged as a promising platform for developing theranostic systems [109,110]. Self-assembly of GSH-stabilized Au nanoclusters (Au-GSH NCs) can be smoothly conducted by employing cationic polymer poly(allyl amine hydrochloride) (PAH) as mediator, and corresponding Au NPs with a mean diameter size of 120 nm were readily constructed [111]. As depicted in **Figure 21**, cross-linking of Au-GSH NCs leads to fluorescence quantum yield enhancement from 7% to 25%, suggesting typical AEE features. The NPs exhibited pH-dependent swelling and shrinking properties in the pH range of 6 to 10, probably resulting from Coulombic interactions between Au-GSH NCs and PAH. To investigate the drug delivery property of this Au NCs system, peptides and antibodies were employed as the substrates for *in vitro* experiments. The results showed that the cellular uptake capability of Au NPs was much better than that of free Au NCs. In comparison to free biomolecules, 1.7-fold and 6.5-fold enhanced cellular uptake of peptides and antibodies were detected by using the Au NPs as drug carriers. Their high brightness, good biocompatibility, excellent stability and remarkable drug-carrying property make these presented Au NPs powerful for theranostic applications [111].

Ingenious use of AIE-based theranostic system is capable of achieving drug distribution monitoring. It has been reported that TPE-DOX NPs can be simply fabricated *via* electrostatic interactions between TPE NPs and DOX [112,113]. Liang's group [114] demonstrated that spatiotemporal visualization of DOX distribution could be successfully performed by using self-indicating TPE-DOX NPs based on different emission colors of TPE NPs, DOX and TPE-DOX NPs. As shown in **Figure 22**, by applying this self-indicating drug delivery system, drug distribution monitoring and release can be easily realized by observing the

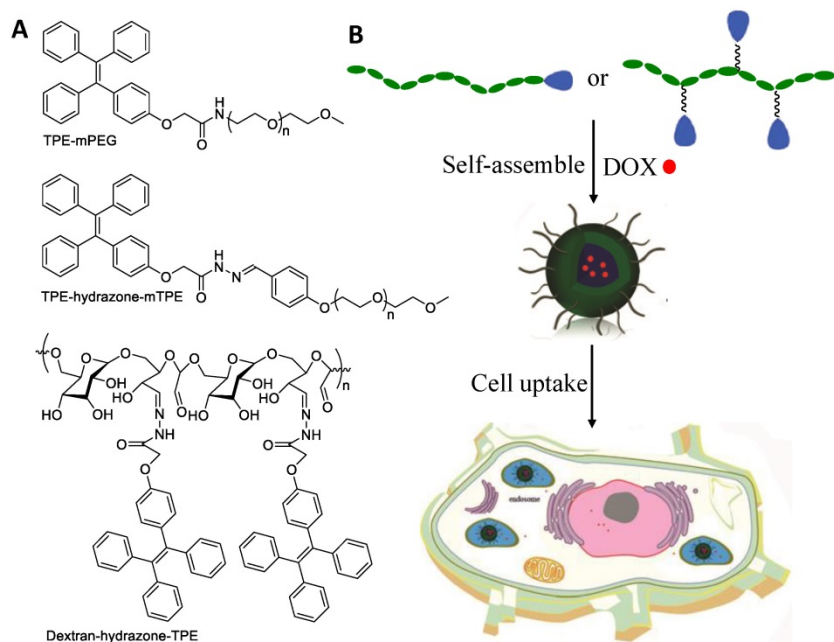


**Figure 20.** Illustration of a drug-loaded micelle with AIE properties as a theranostic platform for intracellular imaging and cancer treatment. Reproduced with permission from [105], copyright 2015 Royal Society of Chemistry.

transition of those different colors in fluorescence microscopy images. TPE-DOX NPs with purple color were first taken up by cells and located in lysosomes, in which pH-sensitive DOX detached from TPE-DOX NPs due to the low internal pH microenvironment. The released DOX in red color escaped from the lysosomes and entered the nuclei, which is the site for DOX therapeutic activity. Meanwhile, blue-emissive TPE NPs without loaded DOX remained in the cytoplasm. The therapeutic effect of TPE NPs, DOX and TPE-DOX NPs was further evaluated by MTT assay of MCF-7s breast cancer cells, and showed that TPE NPs exhibited negligible cytotoxicity even at a concentration as high as 100  $\mu$ M. Moreover, TPE-DOX NPs provided better performance in terms of inhibiting proliferation of cancer cells than free DOX due to the higher concentration of DOX in TPE-DOX NPs-treated cells than that of free DOX-treated cells, indicating their effective drug delivery property. The authors demonstrated that the improved drug delivery efficiency can be attributed to efficient interaction between cell membrane and TPE-DOX NPs with high lipophilicity.

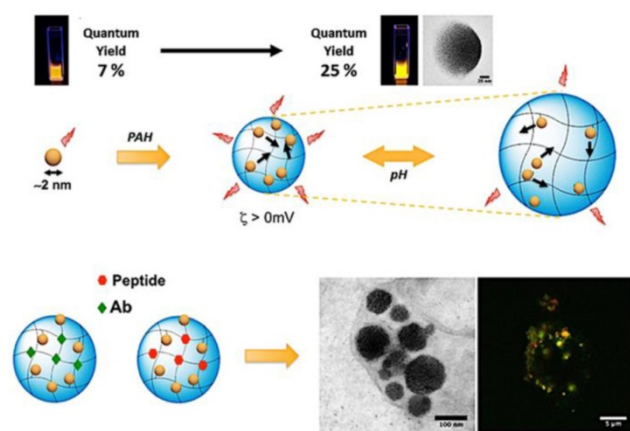


**Figure 21.** Self-assembled gold nanoclusters for bright fluorescence imaging and enhanced drug delivery. Reproduced with permission from [111], copyright 2016 American Chemical Society.

Side effects of drugs are one of the limitations of chemotherapeutic drugs in clinical applications. The use of non-toxic prodrugs with latent cytotoxic activity has been recognized to be a useful strategy to address this limitation [115]. Exploration of a system that can simultaneously realize accurate delivery of the prodrugs to cancer cells, monitoring of prodrugs delivery, drug activation in cancer cell microenvironment and real-time monitoring of drug activation is highly desirable for cancer theranostics. To achieve this goal, conjugation of the prodrug with a fluorophore targeting ligand through a cancerous microenvironment-responsive linker is a commonly used protocol. With aid of the targeting ligand and responsive linker, prodrugs can specifically

accumulate in cancer cells or tumor, and subsequently be activated, while the fluorescence change can be observed upon drug activation, offering a semi-quantitative readout of active drugs.

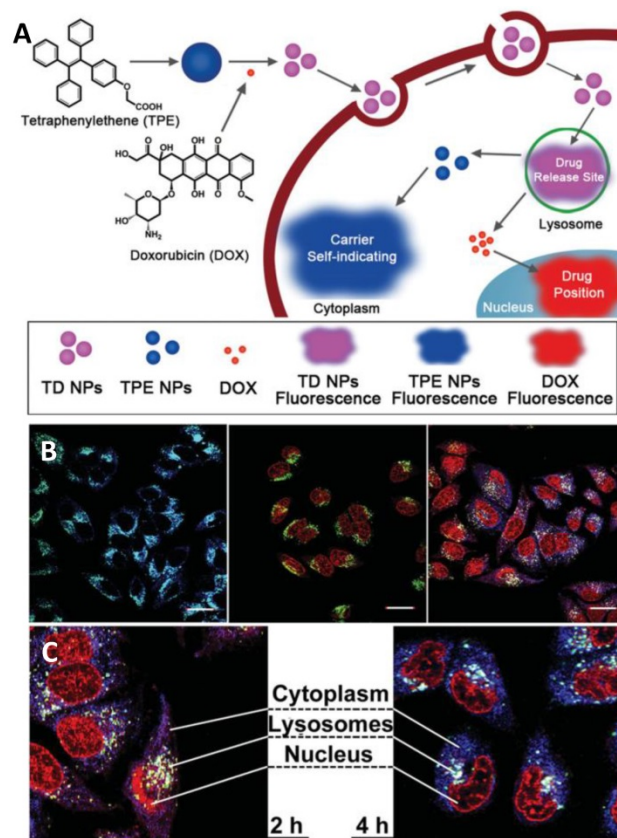


**Figure 22.** Schematic illustration showing the formation of TD NPs, and drug release visualized through an AIE-active drug delivery system. (A) Schematic illustration showing the formation of TD NPs, the drug releasing site, and the real sub-cellular positions of TPE NPs and DOX by the color changes of self-indicating drug delivery system (SIDDS). (B) CLSM images of self-indicating TPE NPs, DOX and TD NPs distribution. (C) Detailed TD NPs spatiotemporal distributions in MCF-7s cells. Reproduced with permission from [114], copyright 2014 Wiley-VCH.

Non-toxic Pt(IV) complexes have been used as prodrugs of their Pt(II) counterparts (such as cisplatin) with chemo-drug nature [116]. Tang and Liu et al. [99] developed an AIE-active compound containing Pt(IV) unit, cRGD fragment, AIE moiety, and hydrophilic aspartic acid. This compound was non-emissive in aqueous media due to energy consumption of the excited state through nonradiative pathways, and it was capable of selectively entering integrin-overexpressing cancer cells (MDA-MB-231 cells) thanks to the existence of the cRGD fragment. The presented probe was reduced intracellularly to generate the toxic Pt(II) drug, resulting in decomposition of this probe. Upon decomposition, the released AIE moiety with poor hydrophilicity aggregated in cells and provided strong emission. In the developed system, quantitative analysis of the active drug concentration was straightforwardly achieved, benefiting from the

“light-up” features of AIEgens. Later on, another AIEgen-based theranostic agent containing two prodrugs was further designed and constructed [117]. As shown in **Figure 23**, the agent was comprised of Pt(IV) prodrug, DOX, TPE and cRGD, and exhibited red fluorescence from DOX due to energy transfer from blue-emissive TPE to red-emissive DOX. Upon drug activation in endo/lysosomes, both TPE and DOX were released from the probe, and Pt(IV) prodrug was reduced to cisplatin. Through drug activation, the blue emission of TPE was intensified within 2 h in cytoplasm, and the red fluorescence of DOX was observed within 6 h in nuclei, indicating visual drug activation. More importantly, synergistic anticancer effect was achieved by using these two drugs. The  $IC_{50}$  of this theranostic agent against MDA-MB-231 cells was 0.69 mM, while DOX and cisplatin provided much higher  $IC_{50}$  values of 1.6 and 18.1 mM, respectively. These interesting features including prodrug tracking, real-time drug activation monitoring and synergistic anticancer effect of two drugs made this theranostic agent a powerful cancer therapy [117]. Shin and co-workers [118] developed an AIE-active and activatable prodrug, which was able to selectively target mitochondria of cancer cells driven by triphenylphosphonium group. Interestingly, this prodrug can be activated by NAD(P)H:quinone oxidoreductase-1 (NQO1) enzyme in cells via the cascade reactions involving reduction, cyclization and elimination of quinine. As the result of prodrug activation, AIE scaffold were released and aggregated to

intensely emit light upon photo excitation, remarkably achieving prodrug activation monitoring. In addition, both *in vitro* and *in vivo* results revealed that the use of this AIEgen can synchronously reach sub-organelle-specific targeting, tissue-selective localization, enzymatic activation of drugs and prodrug activation visualization, suggesting an efficient theranostic system [118].

Apart from monitoring drug distribution and prodrug activation, an ideal theranostic agent should also achieve therapeutic response monitoring, which is significantly critical in clinical applications because the function of therapeutic response monitoring enables theranostic agents to in real time evaluate therapeutic regimes *in situ* and further guide therapeutic decisions. So far, MRI is the most widely used clinical method to evaluate the therapeutic effect of cancer therapy. Moreover, MRI is time-consuming and has low sensitivity; thus, it is unsatisfactory for early-stage cancer diagnosis. In this context, AIEgen-based theranostics involving FLI-guided CHT offer a new opportunity for the development of powerful therapeutic agents having the function of therapeutic response monitoring.

It has been demonstrated that cancer cell apoptosis is related to caspase enzyme activation [119], and some AIEgens have been utilized as powerful tools for monitoring cell apoptosis by detecting caspase enzyme activation. These AIEgens, however, cannot be used to accurately estimate therapeutic response to drugs on site, mainly because of the different subcellular locations of probe and drug [120,121].

In this context, Tang and Liu's groups prepared a prodrug containing a Pt(IV) unit, cRGD tripeptide, an AIE-active tetraphenylsilole (TPS) fluorophore and Asp-Glu-Val-Asp (DEVD) (Figure 24) [122]. DEVD is a peptide sequence that can be specifically cleaved by a cysteine protease caspase-3, in which its activation has been recognized to be one of the most popular pathways of therapeutic drug-induced apoptosis. As depicted in Figure 24, the prodrug was able to be delivered to overexpressed  $\alpha_v\beta_3$  integrin on cancer cells because of the specific affinity of cRGD to  $\alpha_v\beta_3$  integrin. Pt(II) drug was then generated by the reduction of Pt(IV) prodrug in cancer cells. Meanwhile, the prodrug decomposed and released the apoptosis sensor TPS-DEVD. The *in situ*-produced Pt(II) drug triggered cell apoptosis

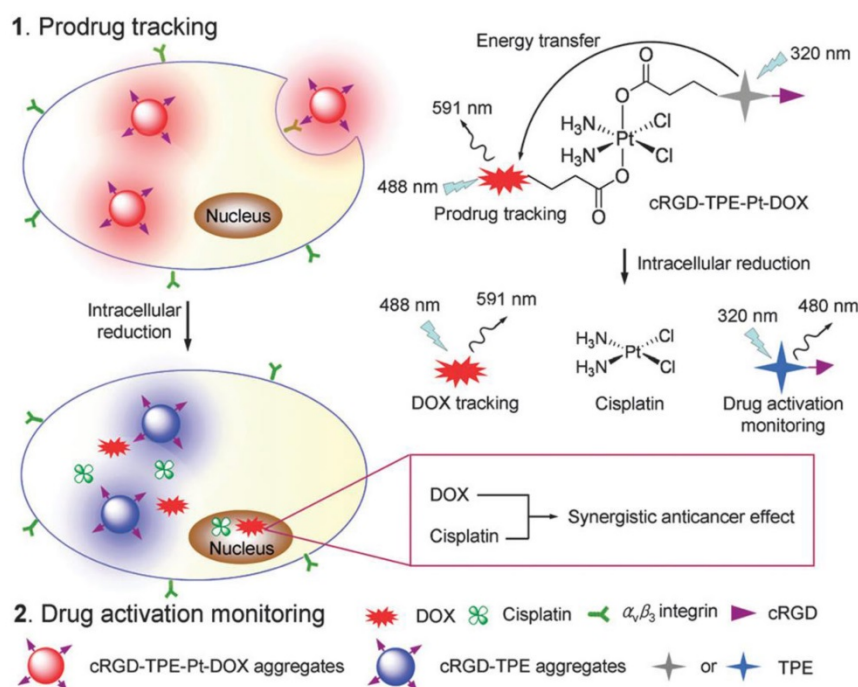


**Figure 23.** Schematic illustration of the targeted theranostic dual-acting prodrug for real-time drug tracking and activation monitoring. Reproduced with permission from [117], copyright 2014 Royal Society of Chemistry.

and activated caspase-3 enzyme to cleave the DEVD peptide sequence. As a result, the hydrophobic TPS moiety was released and aggregated in cells, producing turn-on emission, which can be used for real-time imaging of Pt(II)-induced apoptosis *in situ*, as well as accurate evaluation of therapeutic response to the specific anticancer drug [122]. This report demonstrated a well-designed approach for monitoring drug-induced cellular apoptosis, which opened new opportunities for evaluating therapeutic responses to anticancer drugs.

Aiming to enhance the therapeutic efficiency of drugs, adjuvants have been widely employed in CHT. Tang and Ding's groups [123] reported for the first time an AIE-active adjuvant named TPE-Py-FFGYSA, which was composed of a TPE fragment, FFG tripeptide and a peptide sequence YSAYPDSVPMMS (YSA) (Figure 25). The FFG unit does not only play a role as a linker between TPE and YSA, but is also capable of promoting the AIE performance of TPE-Py-FFGYSA as well, resulting from more efficient restriction of intramolecular motions (RIM) thanks to the existence of an aromatic capping group in FFG. YSA was demonstrated to be a targeting ligand that can selectively bind with EphA2 (a transmembrane receptor tyrosine kinase)-overexpressing cancer cells. Due to its good hydrophilicity, TPE-Py-FFGYSA was weakly emissive in aqueous solution, but its fluorescence was turned on once it specifically

targeted the EphA2-overexpressing prostate PC-3 cancer cells. In a preliminary experiment of cancer cell therapy, Ptx was utilized as a CHT agent, and the IC<sub>50</sub> value was determined to be 75.9 nM. Remarkably, the combination of Ptx with TPE-Py-FFGYSA provided a much lower IC<sub>50</sub> value (7.8 nM) under light irradiation (Figure 25B). In comparison, TPE-Py-FFGYSA alone cannot cause cell death under the same conditions. The authors demonstrated that an intracellular oxidative environment, which was produced by the ROS generation of TPE-Py-FFGYSA upon light illumination, can favor the cytotoxicity enhancement of Ptx against PC-3, thus achieving a synergistic effect of "0 + 1 > 1" [123]. The distinguishing feature of this AIE-active adjuvant could overcome the insensitivity problem of some cancer cells to Ptx drug.

### FLI-guided radiotherapy (RT)

As a first-line therapeutic strategy, radiotherapy (RT), which delivers a high-energy dose of ionizing radiation to the tumor site, has been extensively used as a principle or synergetic tool for therapy of various cancers [124]. However, the resistance of cancer cells to radiation often causes failure of radiotherapy in the clinic [125]. To address this challenging task, scientists have devoted enthusiastic efforts, and found that adjuvants (also called radiosensitizers) are potentially promising because of their capability to make cancer

cells more sensitive to radiotherapy [126]. Chemotherapeutics (such as paclitaxel and cisplatin) and Au NPs are two kinds of radiosensitizers in clinical and research use, but their defects have been recognized. For example, chemotherapeutics commonly cause severe side effects, which make patients suffer; Au NPs exhibit minimal toxicity but lack consensus on the optimum formulation of size and shape, which significantly hinders their clinical translation [127].

Based on the previous work on AIE adjuvant-assisted FLI-guided CHT [123], an AIE-active adjuvant was developed [128], which possesses mitochondrion-specific staining and could efficiently produce ROS with light irradiation. The *in situ*-generated ROS created an intracellular oxidative environment, which was capable of significantly sensitizing cancer cells to ionizing radiation, making the AIEgen (DPA-SCP, in Figure 26A) an

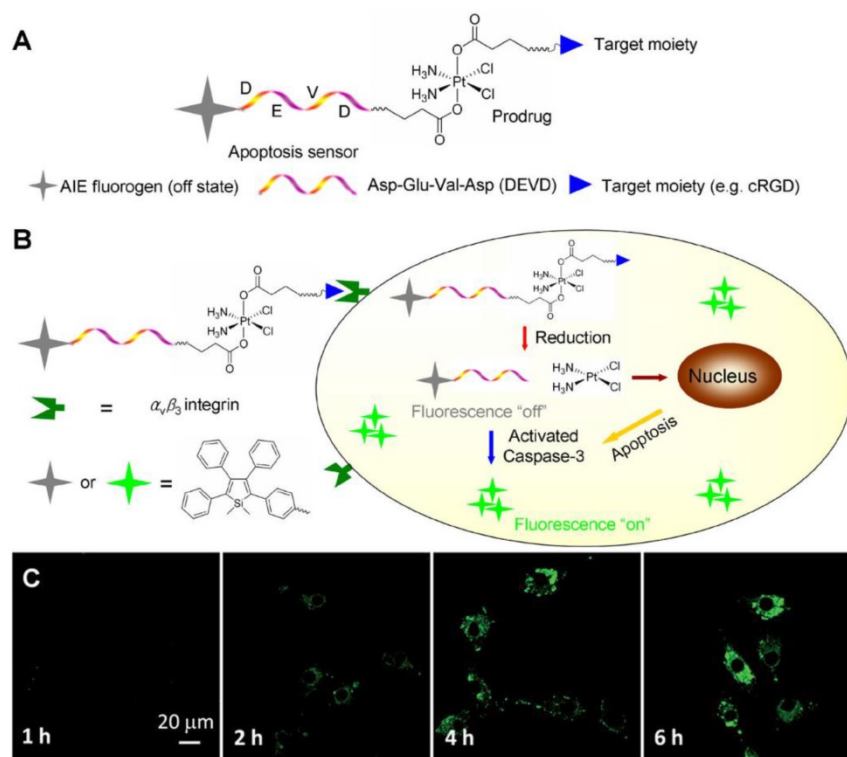


**Figure 24.** (A-B) Schematic illustration of the targeted theranostic platinum(IV) prodrug with a built-in AIE light-up apoptosis sensor for noninvasive *in situ* early evaluation of its therapeutic response. (C) Real-time CLSM images displaying the apoptotic progress of TPS-DEVD-Pt-cRGD-stained U87-MG cells. Reproduced with permission from [122], copyright 2014 American Chemical Society.

outstanding radiosensitizer. DPA-SCP, which was facilely synthesized through a few-steps reaction, was comprised of a pyridinium moiety (working as A), a cyano group (working as A), a carbon-carbon double bond ( $\pi$ -bridge), and a triphenylamine segment (D), which provided extremely high D-A strength. In the structure of DPA-SCP, the pyridinium moiety with positive charge not only played a role as electron accepting unit, but also enabled it to specifically target mitochondria. With white light irradiation, the DPA-SCP accumulated in the mitochondria generated  $^1\text{O}_2$ . Unlike PDT, which involves  $^1\text{O}_2$  generated by AIEgens upon light irradiation resulting in the ablation of cancer cells, in the AIEgen-based

FLI-guided RT application, the generated  $^1\text{O}_2$  from AIEgen did not cause the ablation of cancer cells but rather significantly raised the radiosensitivity of the cancer cells to ionizing radiation, suggesting a synergistic effect of “0 + 1 > 1”. Remarkably, the combination of DPA-SCP and light illumination provided much higher sensitization efficiency of radiotherapy towards A549 cancer cells than both Au NPs and paclitaxel (**Figure 25**) [128]. This successful example of AIE theranostics design will provide a blueprint for the next generation of radiosensitizers for radiotherapy *in vivo*, as well as clinical applications.

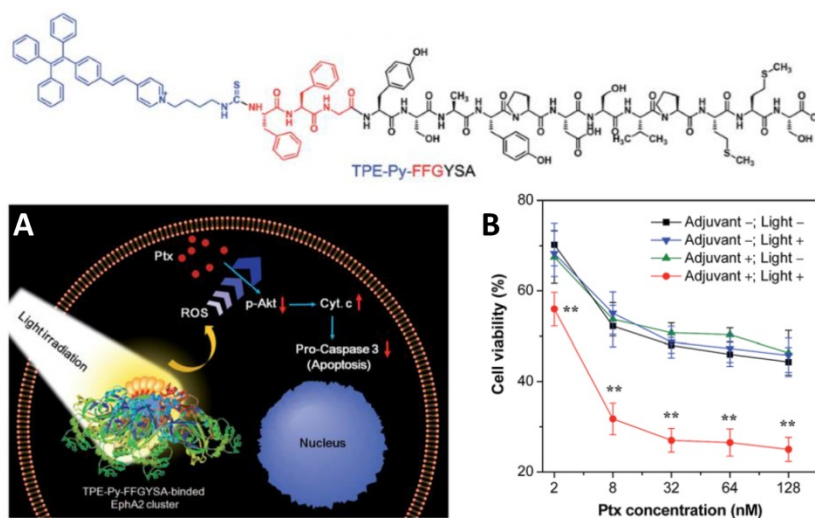


**Figure 25.** (Top) Structure of TPE-Py-FFGYSA. **(A)** Schematic illustration of the proposed synergistic mechanism. **(B)** Cell viabilities of PC-3 cells after the addition of various concentrations of Ptx for 48 h. PC3 cells received different treatments of TPE-Py-FFGYSA (1  $\mu\text{M}$ )/light irradiation. Reproduced with permission from [123], copyright 2017 Royal Society of Chemistry.

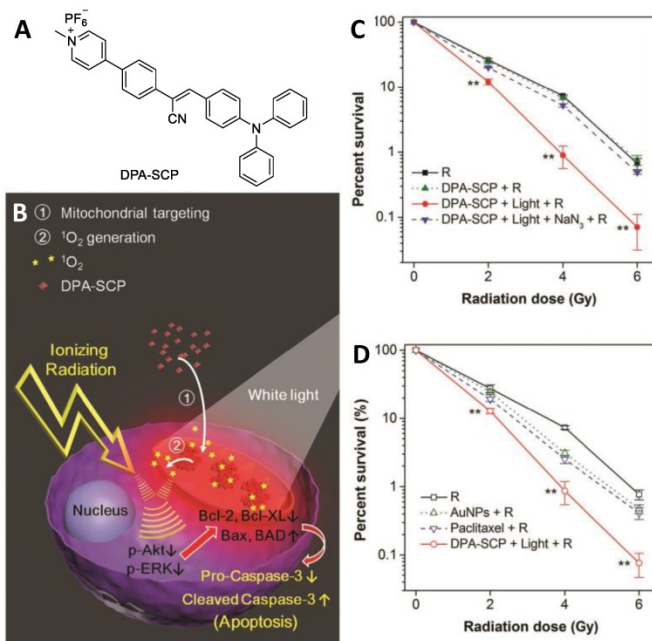


**Figure 26.** **(A)** Structure of DPA-SCP. **(B)** Schematic illustration of the targeted theranostic platinum(IV) prodrug with a built-in AIE light-up apoptosis sensor for noninvasive *in situ* early evaluation of its therapeutic responses. **(C)** Survival curves of A549 cancer cells receiving various treatments as indicated. **(D)** Survival curves of A549 cancer cells pretreated with different radiosensitizers. Reproduced with permission from [128], copyright 2017 Wiley-VCH.

## FLI-guided gene therapy (GT)

Gene therapy has emerged as a promising protocol for cancer treatment through delivering nucleic acid into diseased cells [129]. The vector is one of the key components of a gene therapy system, because it can adequately avoid the nuclease-mediated degradation of nucleic acids, and assist their delivery into cells. To date, various vectors possessing pH-, enzymes-, reducing agents-, or light-responsive features have been widely developed. However, the exploration of vectors with the function of monitorable transfection process, high transfection efficiency and high bio-safety remains challenging [130]. The discovery of AIE opened a new avenue to develop well-performing vectors for gene therapy, because the use of AIE-active vectors would facilitate tracking of gene drug distribution, ensuring accurate drug delivery.

RNA interference (RNAi) has been extensively studied and employed in cancer therapy [131]. In the process of RNAi, a sequence of specific double-stranded RNA is utilized to inhibit gene expression or translation by initiating degradation of a targeted messenger RNA (mRNA) [132]. As ideal alternatives of viral vectors, some NPs have been successfully used as safe carrier systems with high transfection efficiency, while concurrently delivering synthetic small interfering RNAs (siRNAs) into the targeted cells. In this context, some AIEgen-based NPs have been prepared and employed as vectors in gene therapy. Far-red-emissive AIE NPs having high biocompatibility were fabricated by using both Pluronic F127 and PEGylated phospholipid as stabilizers, and applied as nanovectors for gene silencing of mutant K-ras in pancreatic cancer cells [133]. Efficient transfection of siRNA was confirmed

by fluorescence imaging of AIE NPs. Moreover, it was observed that the AIEgen-involving gene therapy system significantly suppressed the expression of the mutant K-ras oncogene from pancreatic cancer cells, suggesting the high potential application of AIE nanovectors for cancer treatment through gene therapy.

Some AIE-active PS-based NPs have been utilized as vectors carrying nucleic acids for gene therapy or synergistic PDT and gene silencing therapy [134,135]. Li and Liu's groups [134] developed a novel nanovector comprising oligoethylenimine (OEI) and PS with both intense red emission and AIE features. These nanovectors can efficiently carry DNA through electrostatic interactions. In addition, with visible light illumination, the generated ROS destroyed the endo/lysosomal membrane. As a result, the unpacking and delivery of DNA were remarkably enhanced, indicating a light-controlled gene delivery system [134]. Later on, a theranostic system involving FLI-guided synergistic PDT and gene silencing therapy was reported by the same group [135]. The theranostic system consisted of an AIE unit (TTD), a small interfering vascular endothelial growth factor (siVEGF), and a cRGD unit (**Figure 27**). It was observed that the siVEGF-TTD NPs were capable of selectively accumulating in  $\alpha_v\beta_3$  integrin-overexpressing cancer cells thanks to the existence of the cRGD unit. Upon light irradiation, the siVEGF-TTD NPs efficiently produced ROS, which ablated cancer cells via a PDT pathway. Meanwhile the VEGF siRNA was carried by the nanovectors and transfected into cancer cells to downregulate VEGF mRNA and protein expressions, offering extraordinary therapeutic efficiency via synergistic PDT-gene therapies [135].

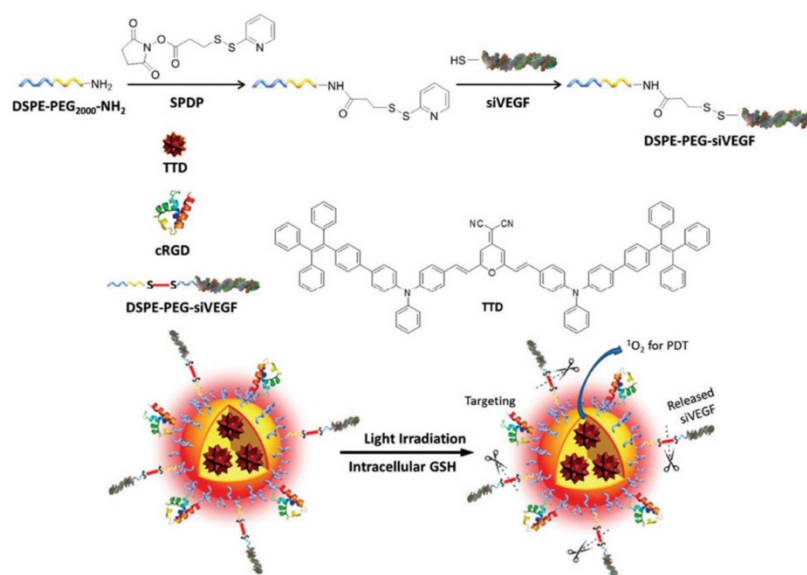


**Figure 27.** Multifunctional theranostic platform involving gene therapy. Reproduced with permission from [135], copyright 2016 Royal Society of Chemistry.

## FLI-guided antibiosis

With the development of human living standards, health issues have captivated much interest. Pathogen prevention and infection treatment are two important branches of healthcare, and antibiotics are the most extensively used reagents for them. Considering the rapid emergence of antibiotic resistance, development of new antibiotics remains an urgently needed and challenging task [136]. AIEgens have in this context emerged as new platforms against drug-resistant bacteria, and have provided promising tools to investigate drug resistance mechanisms.

Tang's group [137] synthesized an orange-emissive positively charged AIEgen, and utilized it for bacteria imaging. It was found that the AIEgen was capable of staining both Gram-positive and -negative bacteria using a 1  $\mu$ M of concentration without the involvement of a washing process, giving high signal-to-noise (S/N) ratio imaging. More importantly, the AIEgen was successfully employed for bacterial susceptibility evaluation and antibiotics screening. The results showed that it was a reliable and effective method, allowing screening completion within 5 h, which was much shorter than that of traditional methods including broth microdilution, disk diffusion and agar dilution [137]. Additionally, it has been reported that a counterpart of this AIEgen named TPE-Bac can not only be used for bacterial imaging with a washing-free procedure, but also for bacteria killing (Figure 28) [138]. TPE-Bac possessed slight dark toxicity towards both Gram-positive and -negative bacteria, which was attributed to damage of membrane integrity caused by intercalation of amphiphilic TPE-Bac into the bacterial membrane. Surprisingly, upon room light irradiation, the bacteria elimination efficiency of TPE-Bac was remarkably

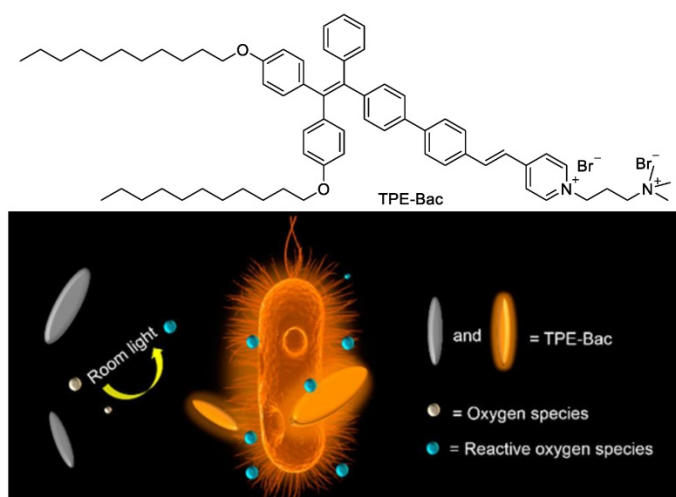


**Figure 28.** Light-enhanced bacterial killing and wash-free imaging based on AIEgen. Reproduced with permission from [138], copyright 2015 American Chemical Society.

enhanced. With the increase of irradiation time, the bacteria viability gradually decreased, and the bacteria elimination was almost complete with room light illumination for 1 h, indicating light-enhanced and -controllable bacteria killing. In the process, TPE-Bac played a role as a PS to generate ROS, which resulted in the efficient bacteria elimination. It is believed that this report offered a novel direction for developing new antibiotics, as well as a promising pathway against drug-resistant bacteria [138].

In another report, Xie and Ramström et al. [139] designed and synthesized an antibacterial compound with AIE characteristics. The compound having twisted structure contained ciprofloxacin, a perfluoroaryl ring, and a phenyl ring linked by an amidine bond. The assembled nano-aggregates of this AIEgen exhibited bright emission and performed well in the application of bacteria imaging. Interestingly, these nano-aggregates efficiently caused bacteria elimination, and their bacterial-killing efficiency was one order higher than their molecular counterpart, suggesting aggregation-enhanced antibacterial activity. The authors demonstrated that the promoted antibacterial activity of the nanodrug probably resulted from both enhanced drug uptake and local drug concentration compared with the molecular drug. This AIEgen-based antibacterial system represents a novel theranostic platform for combating antibiotic resistance [139].

## Photoacoustic imaging (PAI)-guided photothermal therapy (PTT)

PAI, which is established on the PA effect, is a very promising noninvasive imaging modality that is able to provide deep tissue penetration with high resolution with millimeter to centimeter imaging depth and high spatial-temporal resolution [140,141].

PAI has been successfully used as a tool in some areas, such as tumor imaging, studying brain hemodynamic changes, visualizing blood vessel structures, and so on [142]. PTT refers to the use of vibrational energy (heat) of excited states for the treatment of various medical conditions, including cancer [143]. It is generally believed that PTT is more powerful than PDT in terms of cancer treatment, because the therapeutic efficiency of PTT is usually higher than PDT, and PTT does not require oxygen to interact with PSs. The combination of PAI and PTT has been proven to be an outstanding modality in cancer theranostics. Up to now, AIEgen-based PAI-guided PTT has been rarely reported.

Liu's group [144,145] has demonstrated that the conjugation of conventional fluorophores with an AIE moiety can significantly enhance the PA

signal, which mainly results from the promoted thermal expansion upon light absorption benefiting from enhanced molecular rotation. BTPETTQ, which was comprised of a 4,9-di-(5-bromothiophen-2-yl)thiadiazolo-quinoxaline (TTQ) core and two TPE fragments, possessed a propeller structure and strong NIR absorption (**Figure 29**) [145]. It was observed that BTPETTQ exhibited an 89 nm red-shift, bringing about more efficient absorption in the NIR range compared with TTQ. In addition, the PA signal of BTPETTQ NPs was 15% higher than that of TTQ NPs, which can be attributed to the propeller structure of the BTPETTQ molecules. Interestingly, the PA signal output of BTPETTQ NPs was determined to be superior to the widely used Au nanorods based on the same mass, in terms of both PA efficiency and photostability upon laser irradiation, indicating the high potential of AIEgen in the field of PAI. Furthermore, BTPETTQ was utilized as a PA agent for sentinel lymph node (SLN) imaging, which is highly desirable during sentinel lymph node biopsy for the detection of breast cancer metastases. As displayed in **Figure 29C-F**, PA signal intensity in the SLN was clearly caught post BTPETTQ NP injection, and the maximum intensity was reached at 10 min after injection, with an imaging depth of 3 mm and resolution of 50  $\mu\text{m}$ . Moreover, the very weak PA signal of the SLN at 90 min post-injection revealed the almost completed clearance of BTPETTQ NPs. The good balance of sufficient retention time and rapid

clearance made BTPETTQ NPs promising for precise spatial localization of SLNs with good bio-safety in clinical applications [145]. Noteworthy, BTPETTQ NPs also have good thermal generation feature with up to 40% photothermal conversion efficiency, endowing these NPs with remarkable performance for PTT application, in which cancer cells were effectively killed with 808 nm laser irradiation. The authors also demonstrated that the photothermal conversion efficiency of TTQ without TPE moiety was much lower than that of BTPETTQ. The results in this report solidly suggested the great potential of AIEgens in theranostics involving PAI-guided PTT [145].

### FLI-guided chemo-photodynamic combination therapy

Aiming to achieve satisfying anticancer efficacy, one trend is combination therapy, which refers to the combination of different therapeutic methods in one platform for improving therapeutic efficiency with minimized side effects. Among various modalities, the combination of PDT and CHT with different therapeutic mechanisms has been proven to possess great potential in clinical applications [146,147].

Liu's group [148] prepared a probe (TPECB-Pt-D5-cRGD) by conjugating AIE-active PS and platinum prodrug with cRGD, and used it for real-time monitoring of drug activation as well as for combinatorial PDT-CHT against cisplatin-resistant cancer cells (**Figure 30**). TPECB-Pt-D5-cRGD was

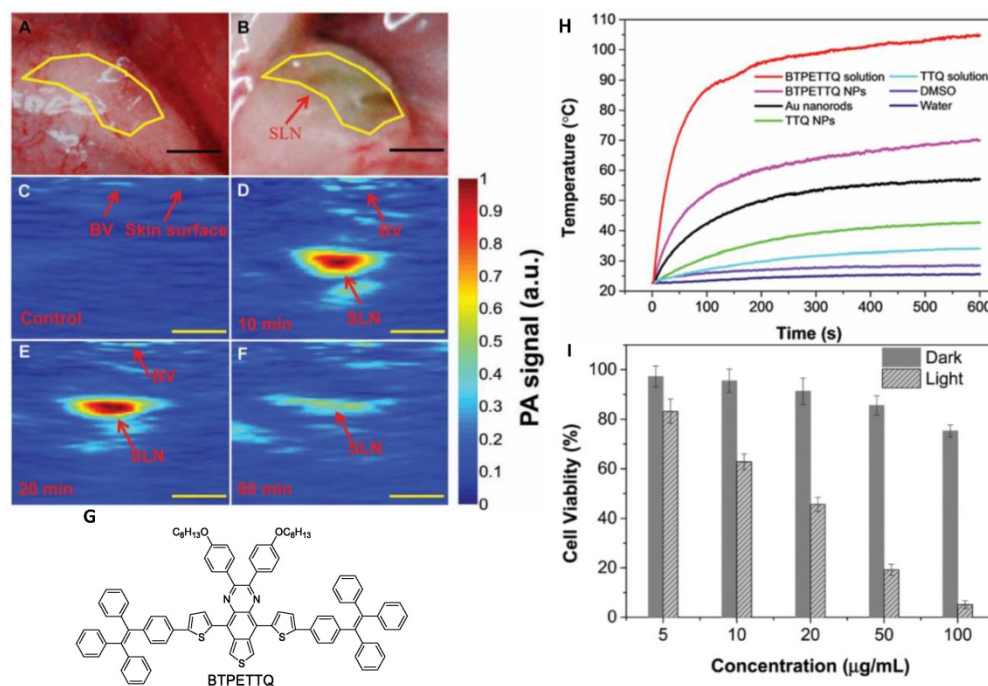


**Figure 29.** PAI-guided PTT. **(A-B)** Hand microscopy images of SLN before (A) and after (B) injection of BTPETTQ NPs. **(C)** Real-time PA imaging of SLN before injection of BTPETTQ NPs. **(D-F)** Real-time PA imaging of SLN 10 min (D), 20 min (E) and 90 min (F) after injection of BTPETTQ NPs. **(G)** Structure of BTPETTQ. **(H)** Temperature evolution of different samples with the same mass concentration after laser irradiation. **(I)** Cell viabilities of HeLa cells after incubation with different concentrations of BTPETTQ NPs-Tat. Reproduced with permission from [145], copyright 2017 Royal Society of Chemistry.

found to be non-emissive in aqueous media but showed bright emission upon reduction by intracellular GSH. With the aid of cRGD, TPECB-Pt-D5-cRGD was capable of selectively staining  $\alpha_v\beta_3$  integrin-overexpressing cancer cells. Subsequently, MTT assays were used to evaluate the anti-proliferative properties of TPECB-PtD5-cRGD in different cells. The results showed that MDA-MB-231 cells were cisplatin resistant with an  $IC_{50}$  value of 33.4  $\mu$ M, and light illumination did not affect the therapeutic efficacy (Figure 30G). The cytotoxicity of TPECB-Pt-D5-cRGD towards MDA-MB-231 cells was similar to that of cisplatin under dark conditions. However, its cytotoxicity was promoted significantly upon light irradiation with a low  $IC_{50}$  of 4.2  $\mu$ M, suggesting the synergetic anti-proliferative effect of TPECB-Pt-D5-cRGD through a combinatorial PDT-CHT pathway (Figure 30H). The presented method involving both platinum prodrug and AIE PS showed the great potential of AIEgen-based materials for cancer theranostics, and opened a novel avenue against CHT resistance.

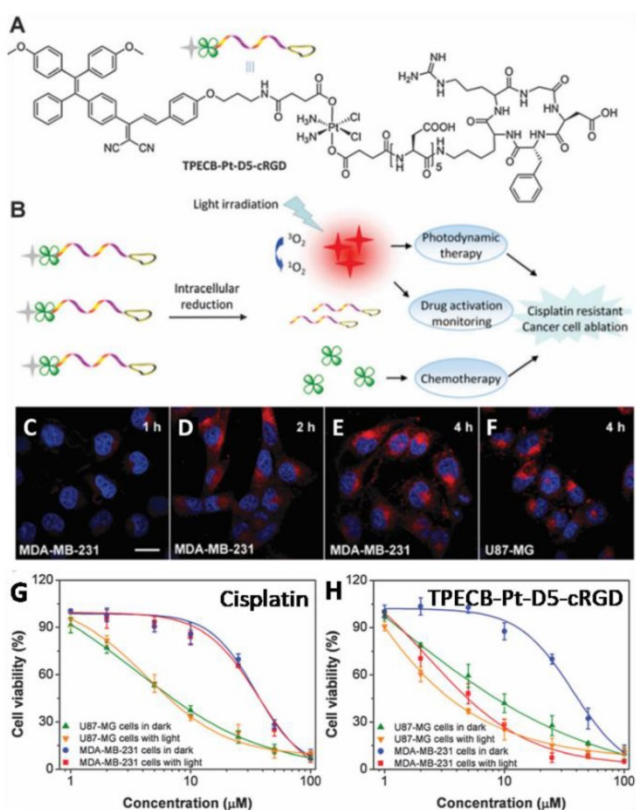


**Figure 30.** Drug activation monitoring and combinatorial photodynamic-CHT against cisplatin-resistant cancer cells using AIEgen. (A) Chemical structure of the prodrug TPECB-Pt-D5-cRGD. (B) Schematic illustration of TPECB-Pt-D5-cRGD used for cisplatin activation monitoring and image-guided combinatorial photodynamic therapy and CHT for the ablation of cisplatin-resistant cancer cells. Confocal images of MDA-MB-231 cells (C–E) and U87-MG cells (F) upon incubation with the prodrug for different time durations. Viability of U87-MG and MDA-MB-231 cells upon incubation with (G) cisplatin or (H) TPECB-Pt-D5-cRGD under dark conditions or under light irradiation. Reproduced with permission from [148], copyright 2015 Royal Society of Chemistry.

## FLI-thermal imaging-guided chemo-photothermal combination therapy

Imaging-guided chemo-photothermal combination therapy is another modality of cancer theranostics containing multiple therapies. It has been demonstrated that photothermal heating could enhance the therapeutic efficiency of CHT, indicating a synergistic method for cancer therapy, because the *in situ*-generated heat is able to facilitate cellular uptake of drugs and/or drug release [149]. Moreover, aiming to achieve precise cancer diagnosis, multimodal imaging is a commonly used strategy, through which the defects of each imaging modality can be avoided or minimized.

Recently, an AIEgen-based theranostic nanoplatform (HSA-PhENH2-PPy-PTX-cRGD) involving FLI-thermal imaging-guided chemo-photothermal combination therapy was designed and prepared [20]. This nanoplatform was comprised of an AIE unit, a cRGD fragment, a PTT agent polypyrrole (PPy) and a CHT agent paclitaxel (PTX). As depicted in Figure 31A, by the use of HSA-PhENH2-PPy-PTX-cRGD NPs, fluorescence imaging of  $\alpha_v\beta_3$ -integrin-positive U87MG tumor was clearly conducted with moderate selectivity and good photo- and thermal stabilities. In contrast, HSA-PhENH2-PPy-PTX without cRGD moiety provided very low accumulation in tumor tissue. It was found that with irradiation by 808 nm laser at 1 W/cm<sup>2</sup>, the average temperature of the tumor region rapidly increased to around 60 °C, and IR thermal mapping of the tumor was clearly observed (Figure 31B), demonstrating dual-modality tumor diagnosis of FLI and thermal imaging. HSA-PhENH2-PPy-PTX NPs without cRGD provided a much lower tumor temperature than HSA-PhENH2-PPy-PTX-cRGD NPs as a result of the low tumor accumulation of HSA-PhENH2-PPy-PTX NPs. Furthermore, the cancer therapy of HSA-PhENH2-PPy-PTX-cRGD was investigated. As shown in Figure 31C, treatments by both HSA-PhENH2-PPy-PTX-cRGD without laser exposure and HSA-PhENH2-PPy-PTX with 808 nm laser exposure showed moderate therapeutic efficacy. Notably, HSA-PhENH2-PPy-PTX-cRGD NPs were capable of completely inhibiting tumor growth upon 808 nm laser irradiation, indicating efficient cancer therapy through chemo-photothermal combination pathways. In addition, H&E staining revealed that neither significant organ damage nor inflammation was found, suggesting the good bio-compatibility of HSA-PhENH2-PPy-PTX-cRGD NPs. Its good diagnostic ability and excellent therapeutic efficacy made this theranostic system promising for further improving multimodal imaging and imaging-guided cancer treatment [20].

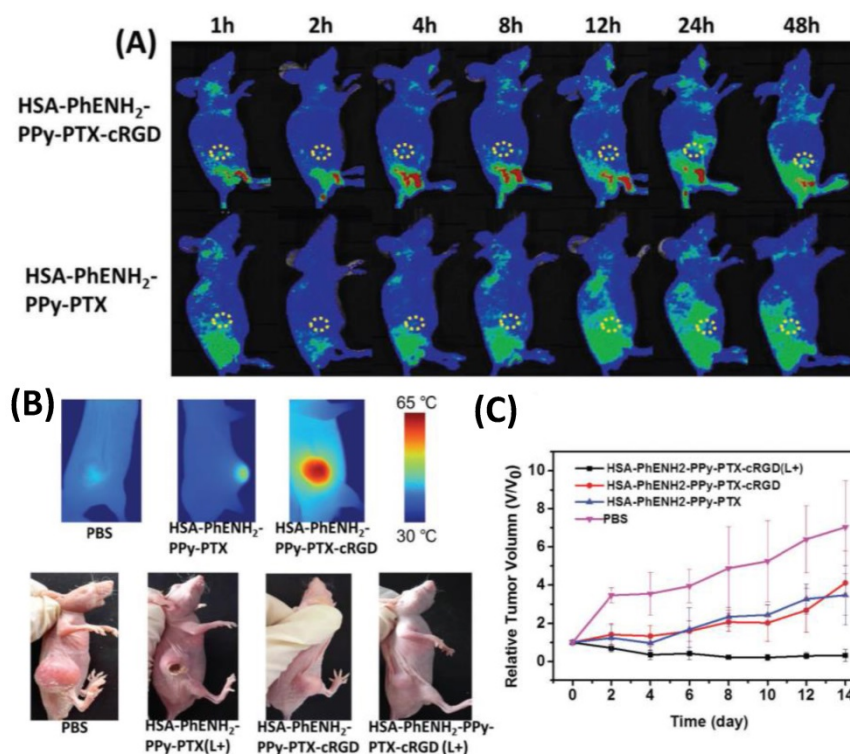


**Figure 31.** Fluorescence-IR thermal imaging-guided chemo-photothermal combination therapy. **(A)** *In vivo* fluorescence images of U87MG tumor-bearing nude mice taken at different time points post injection of HSA-PhENH<sub>2</sub>-PPy-PTX and HSA-PhENH<sub>2</sub>-PPy-PTX-cRGD. **(B)** IR thermal images of U87MG tumor-bearing mice treated with PBS, HSA-PhENH<sub>2</sub>-PPy-PTX, and HSA-PhENH<sub>2</sub>-PPy-PTX-cRGD after exposure to 808 nm laser for 5 min. Representative photographs of mice from different groups taken at the 14<sup>th</sup> day. **(C)** The tumor growth curves of different groups of mice after the above various treatments. Reproduced with permission from [20], copyright 2016 Wiley-VCH.

### FLI and magnetic resonance (MR) dual imaging-guided CHT

As we mentioned in the introduction, the incorporation of FLI and MRI has been recognized to be an ideal protocol for cancer diagnosis. FLI-MRI dual imaging-guided CHT represents a popular design strategy by taking advantage of highly efficient diagnosis and effective therapy. Moreover, supramolecules could be applied in theranostic systems, benefiting from their potential function as nanovectors, multifunctional integration, scalability and facile accessibility [150]. Therefore, it is of interest to develop supramolecular assembly-based theranostic platforms with the function of FLI-MRI dual imaging-guided CHT.

Hu and co-workers [151] utilized the ATRP (atom transfer radical polymerization) technique to prepare block copolymers consisting of pendent epoxy residues within pH-responsive blocks, then a Gd complex and benzaldehyde moieties were conjugated to the copolymers (Figure 32). Micellar NPs were further fabricated by self-assembly of as-synthesized copolymers and TPE-4SH in aqueous solution at neutral pH. Crosslinking was then performed within the micellar cores through thiol-epoxy click reaction between TPE-4SH and epoxy. The crosslinking process endowed the micellar NPs with both long-term stability and intense

fluorescence emission. In addition, the periphery of the micellar NPs was modified with tumor-targetable pH low insertion peptide (pHLIP), forming NPs with a pH-dependent cellular internalization performance. The nanotheranostic platform was finally constructed through encapsulation of the therapeutic drug camptothecin (CPT). It was found that the CPT release was pH-dependent, and acidic microenvironment facilitated the release process by pH-induced hydrophobic-to-hydrophilic transition of the micelle cores. Owing to the TPE units and Gd complex, the micelle-based theranostic nanovector exhibited fluorescence and MR dual imaging capabilities. FLI revealed that the nanovectors can be efficiently taken up by A549 cells thanks to their tumor-targeting capability. On the other hand, the MRI intensity of the nanovectors was approximately  $16.97 \text{ mM}^{-1}\text{s}^{-1}$ , which was 5.4-fold that of the small molecule precursor, indicating aggregation-induced signal enhancement. Moreover, CPT release was efficiently triggered by intracellular acidic pH and provided high efficiency cancer cell killing. Interestingly, *in vivo* MRI investigation displayed that the theranostic nanovectors had enhanced accumulation in tumor tissues, which can be attributed to the conformation change of pHLIP targeting moieties promoted by the extracellular acidic pH of tumor tissues [147]. Although its complicated preparation would impede

practical application, the presented supramolecular assembly-based theranostic platform featuring fluorescence and MR dual modality imaging capability and CHT could provide valuable insights into the design of theranostic systems for clinical uses.

### Switchable FLI-PAI-guided surgery and PDT

Considering the complementary advantages of FLI and PAI, their integration in a single platform with switchable imaging modality would be significantly important by virtue of the potential high sensitivity and imaging depth beyond the optical diffusion limit, but remains challenging.

In this context, Tang's group [152] has designed and synthesized a compound (DTE-TPECM) containing a dithienylethene (DTE) core and 2-(1-(4-(1,2,2-triphenylvinyl)phenyl)ethylidene)malononitrile (TPECM) units, having closed-ring and open-ring isomers (**Figure 33**). Upon external UV light irradiation, closed-ring DTE-TPECM isomer (RClosed-DTE-TPECM) switches to its open-ring counterpart (ROpen-DTE-TPECM), and external visible light irradiation makes ROpen-DTE-TPECM convert back to RClosed-DTE-TPECM, demonstrating controllable structure transformation triggered by external light. As depicted in **Figure 33B**, due to its relatively planar geometric structure with good conjugation, thermal deactivation pathway dominates the excitonic energy consumption of RClosed-DTE-TPECM, while the thermal deactivation of ROpen-DTE-TPECM is blocked, providing intense fluorescence emission. It was observed that RClosed-DTE-TPECM NPs modified by a peptide

with the sequence YSAYPDSVPMMS (YSA) was capable of selectively targeting tumor and giving noticeable PA signal output. In addition, light irradiation with a maximum emission peak at 610 nm efficiently triggered the transformation of RClosed-DTE-TPECM-YSA NPs to ROpen-DTE-TPECM-YSA NPs inside cancer cells, and performed FLI and PDT well. By using PAI, FLI and PDT, total tumor removal was achieved by imaging-guided surgery and PDT. In this study, the authors reported the first case of light-driven switchable FLI-PAI-involving cancer theranostics, and demonstrated a 'one-for-all' system with function-transformable features and utmost effectiveness of each function [152]. This research also explored a pathway for AIEgen-based precision medical treatment with high efficiency.

### Conclusions and outlook

As shown here, theranostics based on AIEgens is a rapidly growing field in the context of both the high demands for theranostics and various distinct advantages of AIEgens. To date, significant breakthroughs and developments of AIEgens-involved theranostic systems have been achieved in the past few years. This great progress was witnessed in several modalities of theranostics, such as FLI-guided PDT, CLI-guided PDT, FLI-guided CHT, FLI-guided RT, FLI-guided GT, FLI-guided antibiosis, PAI-guided PTT, FLI-guided combinational CHT-PDT, FLI-thermal imaging-guided combinational CHT-PTT, FLI-MRI-guided CHT, and switchable FLI-PAI-guided surgery and PDT. In these applications, AIEgens usually exhibit good

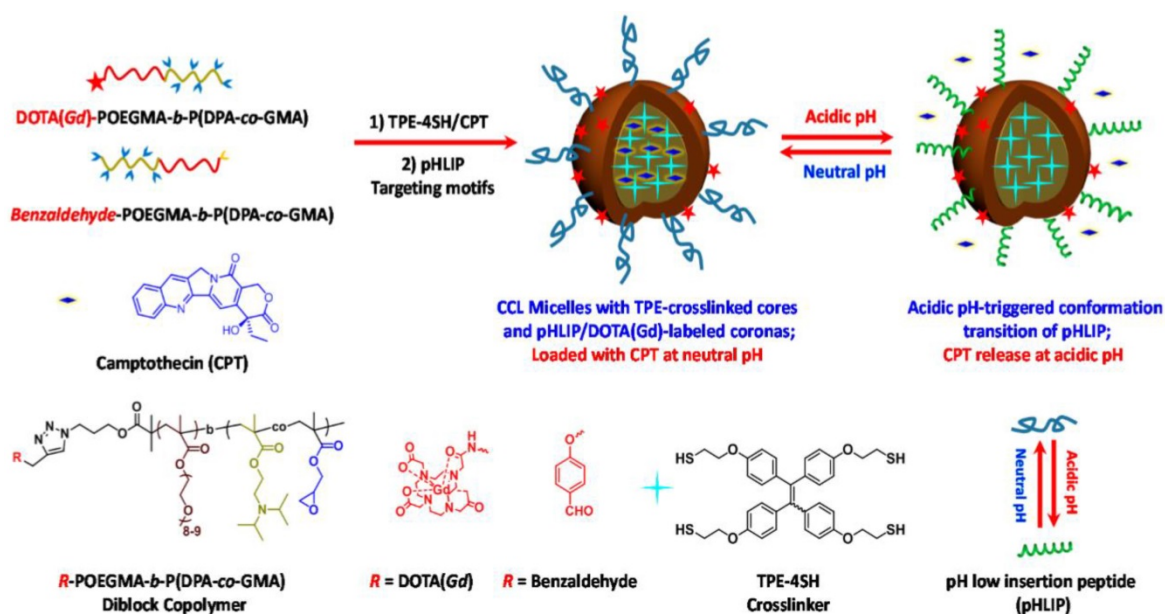


**Figure 32.** pH-responsive tumor-targetable theranostic nanovectors based on core crosslinked (CCL) micelles with fluorescence and MR dual imaging modalities and drug delivery performance. Reproduced with permission from [151], copyright 2016 Multidisciplinary Digital Publishing Institute.

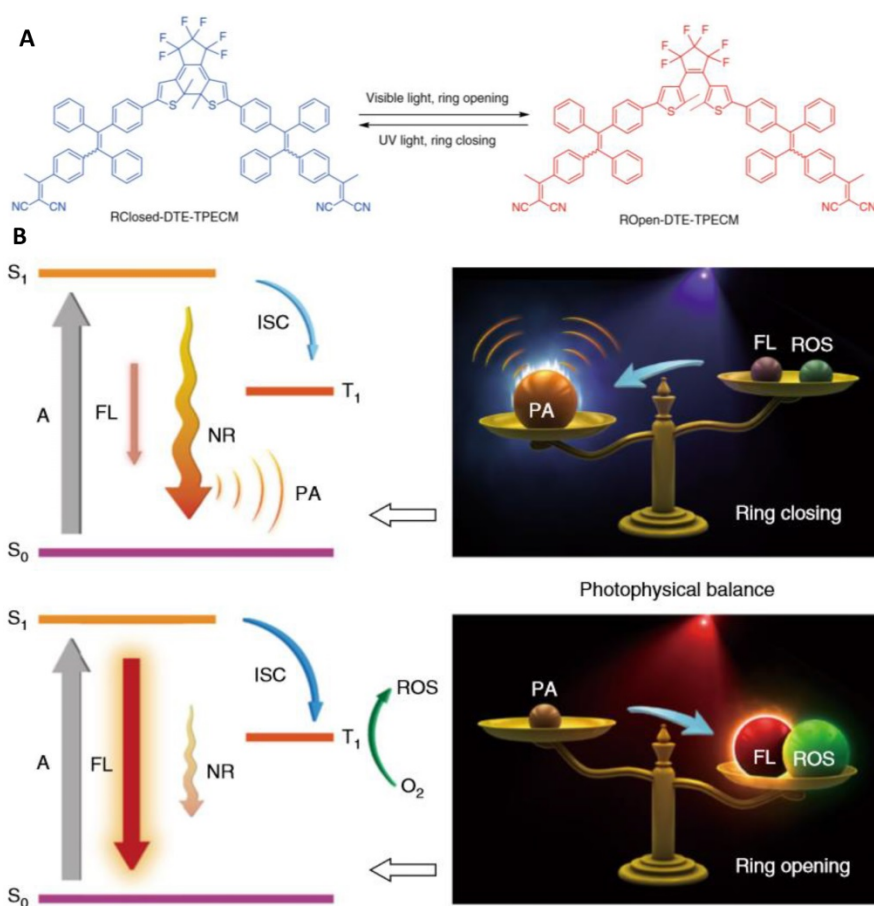


**Figure 33.** Switchable FLI-PAI-guided surgery and PDT. **(A)** Photo-controlled reversibility of DTE-TPECM molecules. **(B)** Illustration of the controllable photophysical processes. Reproduced with permission from [152], copyright 2018 Nature Publishing Group.

biocompatibility, excellent fluorescence properties, promoted efficiencies of photodynamic and photothermal therapies, efficient photoacoustic imaging, and suitability for constructing multimodal imaging and therapy, remarkably indicating the effect of “aggregation-induced theranostic enhancement” (AITE). Consequently, AIEgens hold great potential for theranostics in clinical applications [153].

Although remarkable progress has been made using AIEgens in theranostics, many unsolved problems and challenges remain in many reported results. For instance, a detailed understanding of the structure-property relationships of AIEgens for theranostic uses is still required in order to guide the future design of molecules with desirable functions. Development of new AIEgens with long-wavelength absorption and emission for *in vivo* study is a challenging goal. Extension of the scope of stimuli-responsive turn-on theranostics based on AIEgens is also called for. Expansion of the diversities of multi-modality diagnostic imaging and therapy with good complementation is still expected. The use of AIEgens for multiphoton imaging and therapy is so far underdeveloped. AIE-active theranostic platforms having all functions of drug distribution monitoring,

drug activation monitoring, and therapeutic response monitoring are urgently needed. Further work is also required to seek new imaging systems (for example, AIEgens with room temperature phosphorescence features) [154], to realize specific cancer cell targeting and more effective therapy (for example, conjugation of antibody drugs with AIE-active PSs to achieve antibody-targeted phototherapy against specific cancer cells), and to reach ultrafast imaging and drug delivery [155]. Moreover, attempts to measure their toxicology and clinical evaluations of AIE theranostics should be encouraged. Additionally, compared with conventional theranostic materials, the working concentration of AIEgen-based theranostic platforms is generally high, making AIEgens unfavorable for *in vivo* or clinical trials. In this context, it has been reported that the working concentration of some recently developed AIE systems is comparative to conventional fluorophores for bio-imaging applications [29,37,77]. Therefore, theranostics using these AIEgens with low working concentration should be further developed.

Nowadays, new discoveries are propelling the field by addressing these challenges. Given the fast development pace of this area with rapid progress

and new perspectives, it is most certainly only a matter of time before theranostics based on AIEgens are realized in clinical uses. It is believed that the concept of AIE will stimulate more research interests in life sciences to biomedical fields.

## Abbreviations

ACQ: aggregation-caused quenching; AIE: aggregation-induced emission; AIEgens: AIE luminogens; CHT: chemotherapy; CLI: Chemiluminescence imaging; EPR: enhanced permeability and retention; FLI: fluorescence imaging; GT: gene therapy; IC<sub>50</sub>: half-maximal inhibitory concentration; ISC: intersystem crossing; MR: magnetic resonance; NIR: near-infrared; NPs: nanoparticles; PAI: photoacoustic imaging; PDT: photodynamic therapy; PSs: photosensitizers; PTT: photothermal therapy; ROS: reactive oxygen species; RT: radiotherapy.

## Acknowledgments

This work was partially supported by the President Fund of Shenzhen University Foundation (848-0000106), the Innovation and Technology Commission (ITC-CNERC14SC01), the National Science Foundation of China (21788102), the National Basic Research Program of China (973 Program: 2013CB834701 and 2013CB834702), and the Research Grants Council of Hong Kong (16301614, 16305015, N\_HKUST604/14 and A-HKUST605/16). B.Z.T. is also grateful for support from the Science and Technology Plan of Shenzhen (JCYJ201602292056 01482).

## Competing Interests

The authors have declared that no competing interest exists.

## References

1. Idée JM, Louguet S, Ballet S, Corot C. Theranostics and contrast-agents for medical imaging: A pharmaceutical company viewpoint. *Quant Imaging Med Surg.* 2013; 3: 292-297.
2. Kumar R, Shin WS, Sunwoo K, Kim WY, Koo S, Bhuniya S, et al. Small conjugate-based theranostic agents: an encouraging approach for cancer therapy. *Chem Soc Rev.* 2015; 44: 6670-6683.
3. Xie J, Lee S, Chen X. Nanoparticle-based theranostic agents. *Adv Drug Deliv Rev.* 2010; 62: 1064-1079.
4. Muthu MS, Leong DT, Mei L, Feng SS. Nanotheranostics-application and further development of nanomedicine strategies for advanced theranostics. *Theranostics.* 2014; 4: 660-677.
5. Lammers T, Aime S, Hennink WE, Storm G, Kiessling F. Theranostic nanomedicine. *Acc Chem Res.* 2011; 44: 1029-1038.
6. Ryu JH, Lee S, Son S, Kim SH, Leary JF, Choi K, et al. Theranostic nanoparticles for future personalized medicine. *J Control Release.* 2014; 190: 477-484.
7. Mura A, Couvreur P. Nanotheranostics for personalized medicine. *Adv Drug Deliv Rev.* 2012; 64: 1394-1416.
8. Kim J, Piao Y, Hyeon T. Multifunctional nanostructured materials for multimodal imaging, and simultaneous imaging and therapy. *Chem Soc Rev.* 2009; 38: 372-390.
9. Bardhan R, Lal S, Joshi A, Halas N. Theranostic nanoshells: from probe design to imaging and treatment of cancer. *Acc Chem Res.* 2011; 44: 936-946.

10. Ho YP, Leong KW. Quantum dot-based theranostics. *Nanoscale.* 2010; 2: 60-68.
11. Chen W, Zhang S, Yu Y, Zhang H, He Q. Structural-engineering rationales of gold nanoparticles for cancer theranostics. *Adv Mater.* 2016; 28: 8567-8585.
12. Yu Y, Mok BYL, Loh XJ, Tan YN. Rational design of biomolecular templates for synthesizing multifunctional noble metal nanoclusters toward personalized theranostic applications. *Adv Healthcare Mater.* 2016; 5: 1844-1859.
13. Augustine S, Singh J, Srivastava M, Sharma M, Das A, Malhotra BD. Recent advances in carbon based nanosystems for cancer theranostics. *Biomater Sci.* 2017; 5: 901-952.
14. Xie J, Jon S. Magnetic nanoparticle-based theranostics. *Theranostics.* 2012; 2: 122-124.
15. Wang Z, Niu G, Chen X. Polymeric materials for theranostic applications. *Pharm Res.* 2014; 31: 1358-1376.
16. Feng Y, Panwar N, Tng DJH, Tjin SC, Wang K, Yong KT. The application of mesoporous silica nanoparticle family in cancer theranostics. *Coord Chem Rev.* 2016; 319: 86-109.
17. Feng G, Liu B. Multifunctional AIEgens for future theranostics. *Small.* 2016; 12: 6528-6535.
18. Qi J, Fang Y, Kwok RTK, Zhang X, Hu X, Lam JWY, et al. Highly stable organic small molecular nanoparticles as an advanced and biocompatible phototheranostic agent of tumor in living mice. *ACS Nano.* 2017; 11: 7177-7188.
19. Mei J, Leung NLC, Kwok RT, Lam JW, Tang BZ. Aggregation-induced emission: together we shine, united we soar. *Chem Rev.* 2015; 115: 11718-11940.
20. Wang K, Fan X, Zhao L, Zhang X, Zhang X, Li Z, et al. Aggregation induced emission fluorogens based nanotheranostics for targeted and imaging-guided chemo-photothermal combination therapy. *Small.* 2016; 12: 6568-6575.
21. Gu X, Kwok RTK, Lam JWY, Tang BZ. AIEgens for biological process monitoring and disease theranostics. *Biomaterials.* 2017; 146: 115-135.
22. Liang J, Tang BZ, Liu B. Specific light-up bioprobes based on AIEgen conjugates. *Chem Soc Rev.* 2015; 44: 2798-2811.
23. Luo J, Xie Z, Lam JW, Cheng L, Chen H, Qiu C, et al. Aggregation-induced emission of 1-methyl-1,2,3,4,5-pentaphenylsilole. *Chem Commun.* 2001; 1740-1741.
24. Mei J, Hong Y, Lam JW, Qin A, Tang Y, Tang BZ. Aggregation-induced emission: the whole is more brilliant than the parts. *Adv Mater.* 2014; 26: 5429-5479.
25. Kwok RT, Leung CW, Lam JW, Tang BZ. Biosensing by luminogens with aggregation-induced emission characteristics. *Chem Soc Rev.* 2015; 44: 4228-4238.
26. Hong Y, Lam JWY, Tang BZ. Aggregation-induced emission. *Chem Soc Rev.* 2011; 40: 5361-5388.
27. Gao M, Yu F, Lv C, Choo J, Chen L. Fluorescent chemical probes for accurate tumor diagnosis and targeting therapy. *Chem Soc Rev.* 2017; 46: 2237-2271.
28. Lou X, Zhuang Y, Zou X, Jia Y, Hong Y, Min X, et al. Real-time, quantitative lighting-up detection of telomerase in urines of bladder cancer patients by AIEgens. *Anal Chem.* 2015; 87: 6822-6827.
29. Wang D, Su H, Kwok RTK, Hu X, Zou H, Luo Q, et al. Rational design of a water-soluble NIR AIEgen, and its application in ultrafast wash-free cellular imaging and photodynamic cancer cell ablation. *Chem Sci.* 2018; 9: 3685-3693.
30. Cheng Y, Dai J, Sun C, Liu R, Zhai T, Lou X, et al. Intracellular H<sub>2</sub>O<sub>2</sub>-responsive AIEgen with peroxidase-mediated catalysis for inflammatory cell selective imaging and inhibition. *Angew Chem Int Ed.* 2018; 57: 3123-3127.
31. Zhang X, Lou X, Xia F. Advances in the detection of telomerase activity using isothermal amplification. *Theranostics.* 2017; 7: 1847-1862.
32. Wu Q, Deng C, Peng Q, Niu Y, Shuai Z. Quantum chemical insights into the aggregation induced emission phenomena: a QM/MM study for pyrazine derivatives. *J Comput Chem.* 2012; 33: 1862-1869.
33. Mei J, Wang Y, Tong J, Wang J, Qin A, Sun JZ, et al. Discriminatory detection of cysteine and homocysteine based on dialdehyde-functionalized aggregation-induced emission fluorophores. *Chem Eur J.* 2013; 19: 613-620.
34. Zhao N, Li M, Yan Y, Lam JWY, Zhang YL, Zhao YS, et al. A tetraphenylethene-substituted pyridinium salt with multiple functionalities: synthesis, stimuli-responsive emission, optical wave guide and specific mitochondrion imaging. *J Mater Chem C.* 2013; 1: 4640-4646.
35. Song Z, Zhang W, Jiang M, Sung HHY, Kwok RTK, Nie H, et al. Synthesis of imidazole-based AIEgens with wide color tunability and exploration of their biological applications. *Adv Funct Mater.* 2016; 26: 824-832.

36. Li K, Qin W, Ding D, Tomczak N, Geng J, Liu R, et al. Photostable fluorescent organic dots with aggregation-induced emission (AIE dots) for noninvasive long term cell tracing. *Sci Rep.* 2013; 3: 1150.
37. Wang D, Su H, Kwok RTK, Shan G, Leung ACS, Lee MMSL, et al. Facile Synthesis of red/NIR AIE luminogens with simple structures, bright emissions, and high photostabilities, and their applications for specific imaging of lipid droplets and image-guided photodynamic therapy. *Adv Funct Mater.* 2017; 27: 1704039.
38. Geng J, Liao LD, Qin W, Tang BZ, Thakor N, Liu B. Fluorogens with aggregation induced emission: ideal photoacoustic contrast reagents due to intramolecular rotation. *J Nanosci Nanotechnol.* 2015; 15: 1864-1868.
39. Cai X, Liu J, Liew WH, Duan Y, Geng J, Thakor N, et al. Organic molecules with propeller structures for efficient photoacoustic imaging and photothermal ablation of cancer cells. *Mater Chem Front.* 2017; 1: 1556-1562.
40. Dolmans DEJGJ, Fukumura D, Jian RK. Photodynamic therapy for cancer. *Nat Rev Cancer.* 2003; 3: 380-387.
41. Allison RR, Downie GH, Cuenca R, Hu XH, Childs CJH, Sibata CH. Photosensitizers in clinical PDT. *Photodiagnosis Photodyn Ther.* 2004; 1: 27-42.
42. Ormond AB, Freeman HS. Dye sensitizers for photodynamic therapy. *Materials.* 2013; 6: 817-840.
43. Circu ML, Aw TY. Reactive oxygen species, cellular redox systems, and apoptosis. *Free Radic Biol Med.* 2010; 48: 749-762.
44. Yang L, Wang X, Zhang G, Chen X, Zhang G, Jiang J. Aggregation-induced intersystem crossing: a novel strategy for efficient molecular phosphorescence. *Nanoscale.* 2016; 8: 17422-17426.
45. Feng G, Wu W, Xu S, Liu B. Far red/near-infrared AIE dots for image-guided photodynamic cancer cell ablation. *ACS Appl Mater Interfaces.* 2016; 8: 21193-21200.
46. Xu S, Yuan Y, Cai X, Zhang CJ, Hu F, Liang J, et al. Tuning the singlet-triplet energy gap: a unique approach to efficient photosensitizers with aggregation-induced emission (AIE) characteristics. *Chem Sci.* 2015; 6: 5824-5830.
47. Maeda H, Wu J, Sawa T, Matsumura Y, Hori K. Tumor vascular permeability and the EPR effect in macromolecular therapeutics: a review. *J Controlled Release.* 2000; 65: 271-284.
48. Wu W, Mao D, Hu F, Xu S, Chen C, Zhang CJ, et al. A highly efficient and photostable photosensitizer with near-infrared aggregation-induced emission for image-guided photodynamic anticancer therapy. *Adv Mater.* 2017; 29: 1700548.
49. He T, Niu N, Chen Z, Li S, Liu S, Li J. Novel Quercetin Aggregation-Induced Emission Luminogen (AIEgen) with Excited-State Intramolecular Proton Transfer for In Vivo Bioimaging. *Adv Funct Mater.* 2018; 28: 1706196.
50. Morin PJ. Claudin proteins in human cancer: promising new targets for diagnosis and therapy. *Cancer Res.* 2005; 65: 9603-9606.
51. Schomburg I, Chang A, Placzek S, Söhngen C, Rother M, Lang M, et al. BRENDA in 2013: integrated reactions, kinetic data, enzyme function data, improved disease classification: new options and contents in BRENDA. *Nucleic Acids Res.* 2013; 41: D764-D772.
52. Decock J, Obermajer N, Vozelj S, Hendrickx W, Paridaens R, Kos J. Cathepsin B, cathepsin H, cathepsin X and cystatin C in sera of patients with early-stage and inflammatory breast cancer. *Int J Biol Markers.* 2008; 23: 161-168.
53. Duncan R, Cable H, Kopecek J. Design of oligopeptide side-chains in poly[N-(2-hydroxypropyl)methacrylamide] copolymers to promote efficient degradation by lysosomal enzymes. *Makromol Chem.* 1983; 184: 1997-2008.
54. Ruoslahti E. RGD and other recognition sequences for integrins. *Annu Rev Cell Dev Biol.* 1996; 12: 697-715.
55. Yuan Y, Zhang CJ, Gao M, Zhang R, Tang BZ, Liu B. Specific light-up bioprobe with aggregation-induced emission and activatable photoactivity for the targeted and image-guided photodynamic ablation of cancer cells. *Angew Chem Int Ed.* 2015; 54: 1780-1786.
56. de Iillarduya CT, Düzgünes N. Delivery of therapeutic nucleic acids via transferrin and transferrin receptors: lipoplexes and other carriers. *Expert Opin Drug Delivery.* 2013; 10: 1583-1591.
57. Tortorella S, Karagiannis TC. Transferrin receptor-mediated endocytosis: a useful target for cancer therapy. *J Membr Biol.* 2014; 247: 291-307.
58. Daniels TR, Delgado T, Helguera G, Penichet ML. The transferrin receptor part II: targeted delivery of therapeutic agents into cancer cells. *Clin Immunol.* 2006; 121: 159-176.
59. Gabathuler R. Approaches to transport therapeutic drugs across the blood-brain barrier to treat brain diseases. *Neurobiol Dis.* 2010; 37: 48-57.
60. Zhang R, Feng G, Zhang CJ, Cai X, Cheng X, Liu B. Real-time specific light-up sensing of transferrin receptor: image guided photodynamic ablation of cancer cells through controlled cytomembrane disintegration. *Anal Chem.* 2016; 88: 4841-4848.
61. Weitman SD, Lark RH, Coney LR, Fort DW, Frasca V, Zurawski VR, et al. Distribution of the folate receptor GP38 in normal and malignant cell lines and tissues. *Cancer Res.* 1992; 52: 3396-3401.
62. Paulos CM, Turk MJ, Breue GJ, Low PS. Folate receptor-mediated targeting of therapeutic and imaging agents to activated macrophages in rheumatoid arthritis. *Adv Drug Delivery Rev.* 2004; 56: 1205-1217.
63. Sudimack J, Lee RJ. Targeted drug delivery via the folate receptor. *Adv Drug Delivery Rev.* 2000; 41: 147-162.
64. Feng G, Qin W, Hu Q, Tang BZ, Liu B. Cellular and mitochondrial dual-targeted organic dots with aggregation-induced emission characteristics for image-guided photodynamic therapy. *Adv Healthcare Mater.* 2015; 4: 2667-2676.
65. Lippert AR, De Bittner GCV, Chang CJ. Boronate oxidation as a bioorthogonal reaction approach for studying the chemistry of hydrogen peroxide in living systems. *Acc Chem Res.* 2011; 44: 793-804.
66. Yuan Y, Zhang CJ, Xu S, Liu B. A self-reporting AIE probe with a built-in singlet oxygen sensor for targeted photodynamic ablation of cancer cells. *Chem Sci.* 2016; 7: 1862-1866.
67. Sies H. Glutathione and its role in cellular functions. *Free Radical Biol Med.* 1999; 27: 916-921.
68. Gamcsik MP, Kasibhatla MS, Teeter SD, Colvin OM. Glutathione levels in human tumors. *Biomarkers.* 2012; 17: 671-691.
69. Yuan Y, Zhang CJ, Kwok RTK, Xu S, Zhang R, Wu J, et al. Light-up probe for targeted and activatable photodynamic therapy with real-time *in situ* reporting of sensitizer activation and therapeutic responses. *Adv Funct Mater.* 2015; 25: 6586-6595.
70. Yuan Y, Xu S, Zhang CJ, Zhang R, Liu B. Dual-targeted activatable photosensitizers with aggregation-induced emission (AIE) characteristics for image-guided photodynamic cancer cell ablation. *J Mater Chem B.* 2016; 4: 169-176.
71. Gatenby RA, Gillies RJ. Why do cancers have high aerobic glycolysis? *Nat Rev Cancer.* 2004; 4: 891-899.
72. Gerweck LE, Seetharaman K. Cellular pH gradient in tumor versus normal tissue: potential exploitation for the treatment of cancer. *Cancer Res.* 1996; 56: 1194-1198.
73. Montcourrier P, Silver I, Farnoud R, Bird I, Rochefort H. Breast cancer cells have a high capacity to acidify extracellular milieu by a dual mechanism. *Clin Exp Metastasis.* 1997; 15: 382-392.
74. Yuan Y, Kowk RTK, Tang BZ, Liu B. Smart probe for tracing cancer therapy: selective cancer cell detection, image-guided ablation, and prediction of therapeutic response *in situ*. *Small.* 2015; 11: 4682-4690.
75. Hu Q, Gao M, Feng G, Liu B. Mitochondria-targeted cancer therapy using a light-up probe with aggregation-induced-emission characteristics. *Angew Chem Int Ed.* 2014; 53: 14225-14229.
76. Zhao E, Deng H, Chen S, Hong Y, Leung CWT, Lam JWY, et al. A dual functional AEE fluorogen as a mitochondrial-specific bioprobe and an effective photosensitizer for photodynamic therapy. *Chem. Commun.* 2014; 50: 14451-14454.
77. Gui C, Zhao E, Kwok RTK, Leung ACS, Lam JWY, Jiang M, et al. AIE-active theranostic system: selective straining and killing of cancer cells. *Chem Sci.* 2017; 8: 1822-1830.
78. Kobayashi H, Watanabe R, Choyke PL. Improving conventional enhanced permeability and retention (EPR) effects; What is the appropriate target? *Theranostics.* 2014; 4: 81-89.
79. Han K, Wang SB, Lei Q, Zhu JY, Zhang XZ. Ratiometric biosensor for aggregation-induced emission-guided precise photodynamic therapy. *ACS Nano.* 2015; 9: 10268-10277.
80. Brown S. Two photons are better than one. *Nat Photonics.* 2008; 2: 394-395.
81. Samkoe KS, Clancy AA, Karotki A, Wilson BC, Cramb DT. Complete blood vessel occlusion in the chick chorioallantoic membrane using two-photon excitation photodynamic therapy: implications for treatment of wet age-related macular degeneration. *J Biomed Opt.* 2007; 12: 034025.
82. Alifu N, Dong X, Li D, Sun X, Zebibula A, Zhang G, et al. Aggregation-induced emission nanoparticles as photosensitizer for two-photon photodynamic therapy. *Mater Chem Front.* 2017; 1: 1746-1753.
83. Gu B, Wu W, Xu G, Feng G, Yin F, Chong PHJ, et al. Precise two-photon photodynamic therapy using an efficient photosensitizer with aggregation-induced emission characteristics. *Adv Mater.* 2017; 29: 1701076.
84. Hu L, Xu G. Applications and trends in electrochemiluminescence. *Chem Soc Rev.* 2010; 39: 3275-3304.
85. Gorrini C, Harris IS, Mak TW. Modulation of oxidative stress as an anticancer strategy. *Nat Rev Drug Discov.* 2013; 12: 931-947.
86. Yuan H, Chong H, Wang B, Zhu C, Liu L, Yang Q, et al. Chemical molecule-induced light-activated system for anticancer and antifungal activities. *J Am Chem Soc.* 2012; 134: 13184-13187.

87. Mao D, Wu W, Ji S, Chen C, Hu F, Kong D, et al. Chemiluminescence-guided cancer therapy using a chemically excited photosensitizer. *Chem*. 2017; 3: 991-1007.
88. Ornes S. Antibody-drug conjugates. *Proc Natl Acad Sci USA*. 2013; 110: 13695-13695.
89. Wang S, Huang P, Chen X. Hierarchical targeting strategy for enhanced tumor tissue accumulation/retention and cellular internalization. *Adv Mater*. 2016; 28: 7340-7364.
90. Choi KY, Swierczewska, Chen X, et al. Protease-activated drug development. *Theranostics*. 2012; 2: 156-178.
91. Mura S, Nicolas J, Couvreur P. Stimuli-responsive nanocarriers for drug delivery. *Nat Mater*. 2013; 12: 991-1003.
92. Torchilin VP. Multifunctional, stimuli-sensitive nanoparticulate systems for drug delivery. *Nat Rev Drug Discov*. 2014; 13: 813-827.
93. Yuan Y, Liu B. Visualization of drug delivery processes using AIEgens. *Chem Sci*. 2017; 8: 2537-2546.
94. Yuan Y, Kwok RTK, Zhang R, Tang BZ, Liu B. Targeted theranostic prodrugs based on an aggregation-induced emission (AIE) luminogen for real-time dual-drug tracking. *Chem Commun*. 2014; 50: 11465-11468.
95. Zhao Y, Kwok RTK, Lam JWY, Tang BZ. A highly fluorescent AIE active theranostic agent with anti-tumor activity to specific cancer cells. *Nanoscale*. 2016; 8: 12520-12523.
96. Donnelly LS, Evans DG, Wiseman J, Fox J, Greenhalgh R, Affen J, et al. Uptake of tamoxifen in consecutive premenopausal women under surveillance in a high-risk breast cancer clinic. *Br J Cancer*. 2014; 110: 1681-1687.
97. Shin WS, Park SK, Verwilst P, Koo S, Lee JH, Chi SG, et al. Targeted combinational therapy inducing mitochondrial dysfunction. *Chem Commun*. 2017; 53: 1281-1284.
98. Xue X, Jin S, Zhang C, Yang K, Huo S, Chen F, et al. Probe-inspired nano-prodrug with dual-color fluorogenic property reveals spatiotemporal drug release in living cells. *ACS Nano*. 2015; 9: 2729-2739.
99. Yuan Y, Chen Y, Tang BZ, Liu B. A targeted theranostic platinum(IV) prodrug containing a luminogen with aggregation-induced emission (AIE) characteristics for in situ monitoring of drug activation. *Chem Commun*. 2014; 50: 3868-3870.
100. Han H, Ji Q, Wang Y, Chen Y, Ji J. The rational design of a gemcitabine prodrug with AIE-based intracellular light-up characteristics for selective suppression of pancreatic cancer cells. *Chem Commun*. 2015; 51: 17435-17438.
101. Yua G, Cook TR, Li Y, Yan X, Wu D, Shao L, et al. Tetraphenylethene-based highly emissive metallacage as a component of theranostic supramolecular nanoparticles. *Proc Natl Acad Sci USA*. 2016; 113: 13720-13725.
102. Saha ML, Yan X, Stang PJ. Photophysical properties of organoplatinum(II) compounds and derived self-assembled metallacycles and metallacages: fluorescence and its applications. *Acc Chem Res*. 2016; 49: 2527-2539.
103. Grishagina IV, Pollock JB, Kushal S, Cook TR, Stang PJ, Olenyuk BZ. In vivo anticancer activity of rhomboidal Pt(II) metallacycles. *Proc Natl Acad Sci USA*. 2014; 111: 18448-18453.
104. Zhang C, Jin S, Li S, Xue X, Liu J, Huang Y, et al. Imaging intracellular anticancer drug delivery by self-assembly micelles with aggregation-induced emission (AIE) micelles. *ACS Appl Mater Interfaces*. 2014; 6: 5212-5220.
105. Wang H, Liu G, Gao H, Wang Y. A pH-responsive drug delivery system with an aggregation-induced emission feature for cell imaging and intracellular drug delivery. *Polym Chem*. 2015; 6: 4715-4718.
106. Wang H, Liu G, Dong S, Xiong J, Du Z, Cheng X. A pH-responsive AIE nanoprobe as a drug delivery system for bioimaging and cancer therapy. *J Mater Chem B*. 2015; 3: 7401-7407.
107. Chen Y, Han H, Tong H, Chen T, Wang H, Ji J, et al. Zwitterionic phosphorylcholine-TPE conjugate for pH-responsive drug delivery and AIE active imaging. *ACS Appl Mater Interfaces*. 2016; 8: 21185-21192.
108. Yuan Y, Xu S, Zhang CJ, Liu B. Light-responsive AIE nanoparticles with cytosolic drug release to overcome drug resistance in cancer cells. *Polym Chem*. 2016; 7: 3530-3539.
109. Luo Z, Yuan X, Yu Y, Zhang Q, Leong DT, Lee JY, et al. From aggregation-induced emission of Au(I)-thiolate complexes to ultrabright Au(0)@Au(I)-thiolate core-shell nanoclusters. *J Am Chem Soc*. 2012; 134: 16662-16670.
110. Le Guevel X, Perrino MP, Fernández TD, Palomares F, Torres MJ, Blanca M, et al. Multivalent glycosylation of fluorescent gold nanoclusters promotes increased human dendritic cell targeting via multiple endocytic pathways. *ACS Appl Mater Interfaces*. 2015; 7: 20945-20956.
111. Yahia-Ammar A, Sierra D, Mérola F, Hildebrandt N, Guével XL. Self-assembled gold nanoclusters for bright fluorescence imaging and enhanced drug delivery. *ACS Nano*. 2016; 10: 2591-2599.
112. Zhou Z, Cheng CZ, Zheng Y, Wang Q. Aggregation induced emission mediated controlled release by using a built-in functionalized nanocluster with theranostic features. *J Med Chem*. 2016; 59: 410-418.
113. Jiang BP, Tan X, Shen XC, Lei WQ, Liang WQ, Ji SC, et al. One-step fabrication of a multifunctional aggregation-induced emission nanoaggregate for targeted cell imaging and enzyme triggered cancer chemotherapy. *ACS Macro Lett*. 2016; 5: 450-454.
114. Xue X, Zhao Y, Dai L, Zhang X, Hao X, Zhang C, et al. Spatiotemporal drug release visualized through a drug delivery system with tunable aggregation-induced emission. *Adv Mater*. 2014; 26: 712-717.
115. Rautio J, Kumpulainen H, Heimbach T, Oliyai R, Oh D, Järvinen T, et al. Prodrugs: design and clinical applications. *Nat Rev Drug Discovery*. 2008; 7: 255-270.
116. Graf N, Lippard SJ. Redox activation of metal-based prodrugs as a strategy for drug delivery. *Adv Drug Delivery Rev*. 2012; 64: 993-1004.
117. Yuan Y, Kwok RTK, Zhang R, Tang BZ, Liu B. Targeted theranostic prodrugs based on an aggregation-induced emission (AIE) luminogen for real-time dual-drug tracking. *Chem Commun*. 2014; 50: 11465-11468.
118. Shin WS, Min GL, Verwilst P, Lee JH, Chi SG, Kim JS. Mitochondria-targeted aggregation induced emission theranostics: crucial importance of in situ activation. *Chem Sci*. 2016; 7: 6050-6059.
119. Olsson M, Zhivotovsky B. Caspases and cancer. *Cell Death Differ*. 2011; 18: 1441-1449.
120. Yuan Y, Zhang R, Cheng X, Xu S, Liu B. A FRET probe with AIEgen as the energy quencher: dual signal turn-on for self-validated caspase detection. *Chem Sci*. 2016; 7: 4245-4250.
121. Shi H, Kwok RTK, Liu J, Xing B, Tang BZ, Liu B. Real-time monitoring of cell apoptosis and drug screening using fluorescent light-up probe with aggregation-induced emission characteristics. *J Am Chem Soc*. 2012; 134: 17972-17981.
122. Yuan Y, Kwok RTK, Tang BZ, Liu B. Targeted theranostic platinum(IV) prodrug with a built-in aggregation-induced emission light-up apoptosis sensor for noninvasive early evaluation of its therapeutic responses in situ. *J Am Chem Soc*. 2014; 136: 2546-2554.
123. Chen C, Song Z, Zheng X, He Z, Liu B, Huang X, et al. AIEgen-based theranostic system: targeted imaging of cancer cells and adjuvant amplification of antitumor efficacy of paclitaxel. *Chem Sci*. 2017; 8: 2191-2198.
124. Schae D, McBride WH. Opportunities and challenges of radiotherapy for treating cancer. *Nat Rev Clin Oncol*. 2015; 12: 527-540.
125. Siegel RL, Miller KD, Jemal A. Cancer statistics, 2015. *Ca-Cancer J Clin*. 2015; 65: 5-29.
126. Corde S, Joubert A, Adam JF, Charvet AM, Le BJE, Estève F, et al. Synchrotron radiation-based experimental determination of the optimal energy for cell radiotoxicity enhancement following photoelectric effect on stable iodinated compounds. *Br J Cancer*. 2004; 91: 544-551.
127. Zhang XD, Wu D, Shen X, Chen J, Sun YM, Liu PX, et al. Size-dependent radiosensitization of PEG-coated gold nanoparticles for cancer radiation therapy. *Biomaterials*. 2012; 33: 6408-6419.
128. Yu CYY, Xu H, Ji S, Kwok RTK, Lam JWY, Li X, et al. Mitochondrion-anchoring photosensitizer with aggregation-induced emission characteristics synergistically boosts the radiosensitivity of cancer cells to ionizing radiation. *Adv Mater*. 2017; 29: 1606167.
129. Sheridan C. Gene therapy finds its niche. *Nat Biotechnol*. 2011; 29: 121-128.
130. Yin H, Kanasty RL, Eltoukhy AA, Vegas AJ, Dorkin JR, Anderson DG. Non-viral vectors for gene-based therapy. *Nat Rev Genet*. 2014; 15: 541-555.
131. Peer D, Lieberman J. Special delivery: targeted therapy with small RNAs. *Gene Ther*. 2011; 18: 1127-1133.
132. Nykänen A, Haley B, Zamore PD. ATP requirements and small interfering RNA structure in the RNA interference pathway. *Cell*. 2001; 107: 309-321.
133. Hu R, Yang C, Wang Y, Lin G, Qin W, Ouyang Q, et al. Aggregation-induced emission (AIE) dye loaded polymer nanoparticles for gene silencing in pancreatic cancer and their in vitro and in vivo biocompatibility evaluation. *Nano Res*. 2015; 8: 1563-1576.
134. Yuan Y, Zhang CJ, Liu B. A photoactivatable AIE polymer for light-controlled gene delivery: concurrent endo/lysosomal escape and DNA unpacking. *Angew Chem Int Ed*. 2015; 54: 11419-11423.
135. Jin G, Feng G, Qin W, Tang BZ, Liu B, Li K. Multifunctional organic nanoparticles with aggregation-induced emission (AIE) characteristics for targeted photodynamic therapy and RNA interference therapy. *Chem Commun*. 2016; 52: 2752-2755.
136. Payne DJ. Desperately seeking new antibiotics. *Science*. 2008; 321: 1644-1645.
137. Zhao E, Chen Y, Chen S, Deng H, Gui C, Leung CWT, et al. A luminogen with aggregation-induced emission characteristics for wash-free bacterial imaging, high-throughput antibiotics screening and bacterial susceptibility evaluation. *Adv Mater*. 2015; 27: 4931-4937.
138. Zhao E, Chen Y, Wang H, Chen S, Lam JWY, Leung CWT, et al. Light-enhanced bacterial killing and wash-free imaging based on AIE fluorogen. *ACS Appl Mater Interfaces*. 2015; 7: 7180-7188.
139. Xie S, Manuguri S, Proietti G, Romson J, Fu Y, Inge AK, et al. Design and synthesis of theranostic antibiotic nanodrugs that display enhanced antibacterial activity and luminescence. *Proc Natl Acad Sci USA*. 2017; 114: 8464-8469.

140. Wang LHV, Hu S. Photoacoustic tomography: in vivo imaging from organelles to organs. *Science*. 2012; 335: 1458-1462.
141. Pu K, Shuhendler AJ, Jokerst JV, Mei J, Gambhir SS, Bao Z, et al. Semiconducting polymer nanoparticles as photoacoustic molecular imaging probes in living mice. *Nat Nanotechnol*. 2014; 9: 233-239.
142. Kim C, Favazza C, Wang LHV. In vivo photoacoustic tomography of chemicals: high-resolution functional and molecular optical imaging at new depths. *Chem Rev*. 2010; 110: 2756-2782.
143. Huang X, El-Sayed I, Qian W, Elsayed MA. Cancer cell imaging and photothermal therapy in the near-infrared region by using gold nanorods. *J Am Chem Soc*. 2006; 128: 2115-2120.
144. Geng J, Liao LD, Qin W, Tang BZ, Thakor N, Liu B. Fluorogens with aggregation induced emission: ideal photoacoustic contrast reagents due to intramolecular rotation. *J Nanosci Nanotechnol*. 2015; 15: 1864-1868.
145. Cai X, Liu J, Weng HL, Duan Y, Geng J, Thakor NV, et al. Organic molecules with propeller structures for efficient photoacoustic imaging and photothermal ablation of cancer cells. *Mater Chem Front*. 2017; 1: 1556-1562.
146. Olivo M, Bhuvanewari R, Lucky SS, Dendukuri N, SooPing TP. Targeted therapy of cancer using photodynamic therapy in combination with multi-faceted anti-tumor modalities. *Pharmaceuticals*. 2010; 3: 1507-1529.
147. Zhang CJ, Hu Q, Feng G, Zhang R, Yuan Y, Lu X, et al. Image-guided combination chemotherapy and photodynamic therapy using a mitochondriatargeted molecular probe with aggregation-induced emission characteristics. *Chem Sci*. 2015; 6: 4580-4586.
148. Yuan Y, Zhang CJ, Liu B. A platinum prodrug conjugated with a photosensitizer with aggregation-induced emission (AIE) characteristics for drug activation monitoring and combinatorial photodynamic-chemotherapy against cisplatin resistant cancer cells. *Chem Commun*. 2015; 51: 8626-8629.
149. Yu J, Ju Y, Zhao L, Chu X, Yang W, Tian Y, et al. Multistimuli-regulated photochemothermal cancer therapy remotely controlled via Fe<sub>3</sub>C<sub>2</sub> nanoparticles. *ACS Nano*. 2016; 10: 159-169.
150. Ikkala O, ten Brinke G. Functional materials based on self-assembly of polymeric supramolecules. *Science*. 2002; 295: 2407-2409.
151. Tian S, Liu G, Wang X, Zhang G, Hu J. pH-responsive tumor-targetable theranostic nanovectors based on core crosslinked (CCL) micelles with fluorescence and magnetic resonance (MR) dual imaging modalities and drug delivery performance. *Polymers*. 2016; 8: 226.
152. Qi J, Chen C, Zhang X, Hu X, Ji S, Kowk RTK, et al. Light-driven transformable optical agent with adaptive functions for boosting cancer surgery outcomes. *Nat Commun*. 2018; 9: 1848.
153. Lee MH, Sharma A, Chang MJ, Lee J, Son S, Sessler JL, et al. Fluorogenic reaction-based prodrug conjugates as targeted cancer theranostics. *Chem Soc Rev*. 2018; 47: 28-52.
154. Fatemina SMA, Mao Z, Xu S, Yang Z, Chi Z, Liu B. Organic nanocrystals with bright red persistent room-temperature phosphorescence for biological applications. *Angew Chem Int Ed*. 2017; 56: 12160-12164.
155. Nicol A, Kwok RTK, Chen C, Zhao W, Chen M, Qu J, et al. Ultrafast delivery of aggregation-induced emission nanoparticles and pure organic phosphorescent nanocrystals by saponin encapsulation. *J Am Chem Soc*. 2017; 139: 14792-14799.